Variational Anonymous Quantum Sensing

Muhammad Shohibul Ulum, Uman Khalid, Jason William Setiawan, Trung Q. Duong, *Fellow, IEEE*, Moe Z. Win, *Fellow, IEEE*, and Hyundong Shin, *Fellow, IEEE*

***Abstract*— Quantum sensing networks (QSNs) incorporate quantum sensing and quantum communication to achieve Heisenberg precision and unconditional security by leveraging quantum properties such as superposition and entanglement. However, the QSNs deploying noisy intermediate-scale quantum (NISQ) devices face near-term practical challenges. In this paper, we employ variational quantum sensing (VQS) to optimize sensing configurations in noisy environments for the physical quantity of interest, e.g., magnetic-field sensing for navigation, localization, or detection. The VQS algorithm is variationally and evolutionarily optimized using a genetic algorithm for tailoring a variational or parameterized quantum circuit (PQC) structure that effectively mitigates quantum noise effects. This *genetic* VQS algorithm designs the PQC structure possessing the capability to create a variational probe state that metrologically outperforms the maximally entangled or product quantum state under bit-flip, dephasing, and amplitude-damping quantum noise for both single-parameter and multiparameter NISQ sensing, specifically as quantified by the quantum Fisher information. Furthermore, the quantum anonymous broadcast (QAB) shares the sensing information in the VQS network, ensuring anonymity and untraceability of sensing data. The broadcast bit error probability (BEP) is further analyzed for the QAB protocol under quantum noise, showing its robustness—i.e., *error-free* resilience—against bit-flip noise as well as the *low-noise* BEP behavior. This work provides a scalable framework for integrated quantum anonymous sensing and communication, particularly in a *variational* and *untraceable* manner.**

***Index Terms*— Integrated sensing and communication, quantum anonymous communication, quantum Cramér–Rao bound, variational quantum sensing.**

I. Introduction

QUANTUM SENSING, combined with quantum communication, is poised to revolutionize wireless positioning and sensing technologies by leveraging quantum properties to offer unparalleled precision and security [1], [2]. Wireless positioning and sensing is pivotal for the deployment of next-generation integrated sensing and communication (ISAC) technologies for augmented localization services, environmental monitoring, secure positioning, vehicular safety, real-time precise surveillance, and seamless immersive experiences [3], [4], [5], [6], [7], [8], [9], [10], [11], [12]. These services require ultra-reliable, ultra-secure, and low-latency communications as well as ultra-precise sensing and hyper-accurate measurements [13], [14], [15]. However, classical networks face fundamental limitations in achieving advanced levels of precision and security. For instance, an intrinsic limitation is imposed by the standard quantum limit (SQL), which states that the variance of measurement precision scales as $1/N$ for a network of N sensors [16]. Although this degree of precision is sufficient for diverse real-world applications, emerging fields, such as healthcare networks, augmented reality, virtual reality, gravitational wave detection, and autonomous vehicular networks, require even more precision [17], [18], [19]. Moreover, classical noise such as shot noise, with a variance that typically scales as $1/N$, can further undermine classical sensing networks, thereby reducing their accuracy. In addition, sensing network security based on computational encryption methods is highly prone to quantum attacks owing to perpetual quantum computing capabilities.

Quantum Internet of Things (IoT) incorporates both quantum sensing and quantum communication to further augment sensing and communication capabilities of classical IoT [20], [21], [22], [23]. The emerging paradigm not only improves precision in measuring physical quantities such as electric and magnetic fields but also invokes unconditional communication security by harnessing quantum properties such as superposition and entanglement. Herein, the achievable precision of an entangled quantum sensing network (QSN) is fundamentally limited by the *Heisenberg* limit, exhibiting $1/N^2$ scaling in the measurement precision variance [16], [24]. Nonetheless, deployments of QSNs face hurdles such as the detrimental noise effects on quantum-enhanced precision. Noise sources, e.g., thermal fluctuations and particle loss, can markedly degrade quantum states essential for achieving the Heisenberg-limit precision, necessitating intricate noise mitigation and error correction strategies [25], [26]. In terms of security, post-quantum secure protocols have been posited for QSNs, employing lattice-based cryptographic schemes resilient to quantum attacks [27]. Consequently, quantum IoT embodies a potent platform for high-precision measurements while ensuring robust communication security against quantum

Manuscript received 12 November 2023; revised 19 March 2024; accepted 18 April 2024. Date of publication 14 June 2024; date of current version 21 August 2024. The fundamental research described in this paper was supported, in part, by the National Research Foundation of Korea under Grant 2022R1A4A3033401, by the Information Technology Research Center (ITRC) under Grant IITP-2024-2021-0-02046, by the Canada Excellence Research Chair (CERC) Program CERC-2022-00109, and by the National Science Foundation under Grant CCF-2153230. *(Corresponding author: Hyundong Shin.)*

Muhammad Shohibul Ulum, Uman Khalid, Jason William Setiawan, and Hyundong Shin are with the Department of Electronics and Information Convergence Engineering, Kyung Hee University, Giheung-gu, Yongin-si, Gyeonggi-do 17104, South Korea (e-mail: hshin@khu.ac.kr).

Trung Q. Duong is with the Faculty of Engineering and Applied Science, Memorial University, St. John's, NL A1C 5S7, Canada, and also with the School of Electronics, Electrical Engineering and Computer Science, Queen's University Belfast, Belfast, U.K. (e-mail: tduong@mun.ca).

Moe Z. Win is with the Laboratory for Information and Decision Systems (LIDS), Massachusetts Institute of Technology, Cambridge, MA 02139 USA (e-mail: moewin@mit.edu).

Color versions of one or more figures in this article are available at https://doi.org/10.1109/JSAC.2024.3414932.

Digital Object Identifier 10.1109/JSAC.2024.3414932

threats. However, the limitations of noisy intermediate-scale quantum (NISQ) devices, especially concerning privacy leakage and quantum noise, hinder the full realization of the potential benefits of integrating quantum sensing and communication [28], [29].

Variational quantum sensing (VQS) fully leverages near-term quantum advantages while addressing inherent quantum noise effects as well as quantum device imperfections [30], [31], [32], [33], [34]. VQS algorithms are resource-efficient, taking into account the qubit count, gate depth, and robustness against quantum noise [35]. The VQS algorithms iteratively adjust sensing configurations to optimize quantum sensing probes to precisely estimate physical quantities such as magnetic field, electric field, frequency, and temperature under noisy environments [35]. Employing such an entangled QSN with hybrid quantum-classical optimization exhibits quantum advantage in outperforming classical methods for dynamic sensing environments. In cryptographic metrology, QSNs are designed for specific security-oriented sensing tasks related to secure surveillance, privacy-preserving asset tracking, unauthorized object detection, and anonymous navigation [36], [37]. Herein, the location of stationary sensing nodes and the identity of mobile sensing nodes can become highly relevant in addition to the private data itself. Therefore, the sensing nodes must operate in an anonymous mode while sharing the sensing information or estimated parameters with other network participants. Quantum anonymous communication (QAC) becomes a primary candidate for such scenarios, to ensure sensing anonymity, disapprove unauthorized node access, limit spoofing by blocking malicious nodes, and render the sensing nodes as untraceable [38], [39], [40], [41]. Therefore, such integrated quantum anonymous sensing (QAS) and communication networks can be deployed to deliver improved precision, enhanced sensitivity, and sensing privacy in parallel with classical counterparts.

Specifically, in this paper, we propose an integrated framework incorporating VQS with quantum anonymous broadcast (QAB) for variational QAS networks, as shown in Fig. 1, where a high-quality sensing probe state is prepared by the genetic algorithm (GA) and variational quantum algorithm (VQA) to mitigate the effect of environmental noise. The GA is utilized to find the fittest parameterized quantum circuit (PQC) structure, whereas its angle parameters are optimized variationally. This VQS probe state encodes the unknown parameter of interest. The encoded VQS probe state undergoes quantum measurements, where the obtained measurement outcomes are employed to estimate the unknown parameter. The extracted sensing information is then anonymously broadcast to sensor nodes within the QSN. This involves modulating the sensing information into the shared Greenberger–Horne–Zeilinger (GHZ) state. The modulated information is then extracted by means of quantum measurements performed by all network participants. By harnessing the power of quantum algorithms, VQS optimizes NISQ sensors to mitigate quantum noise effects and enhance measurement precision. In parallel, QAB introduces a privacy layer to QSNs, preserving the anonymity of sensing data. This ISAC framework promises to achieve both quantum-empowered sensing precision and privacy, addressing critical classical

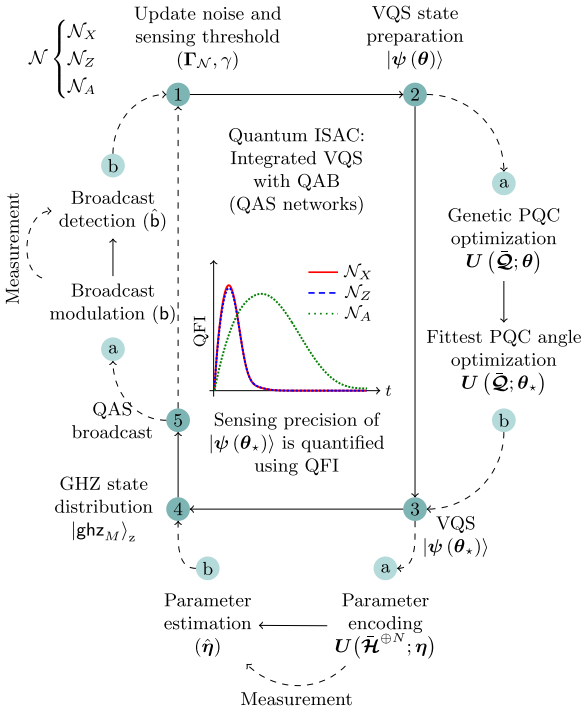

Fig. 1. Quantum anonymous ISAC in a variational and untraceable manner by integrating genetic VQS with QAB. The genetic VQS prepares a high-quality sensing probe state by variationally and evolutionarily finding the tailored PQC structure under quantum noise $\mathcal{N}$. The fittest parameters of the tailored PQC are optimized using classical optimization routines. This genetic VQS probe state interacts with the physical quantity of interest, which is then estimated by quantum measurement. The sensing information is then anonymously shared with other sensing nodes in the network using the QAB protocol. The protocol begins by distributing the GHZ state (broadcast carrier) among the network participants, followed by the broadcast modulation. The QAS broadcast is then recovered by measurements of all network parties. Here, the noisy maps $\mathcal{N}_X$, $\mathcal{N}_Z$, and $\mathcal{N}_A$ stand for bit-flip, dephasing, and amplitude-damping noises, respectively.

constraints in ISAC—with applications in navigation, localization, imaging, and detection (radar), for example. Our main contributions are summarized in the following.

- We introduce quantum sensing protocols and VQAs to formally define VQS protocols for single-parameter and multiparameter sensing tasks in noisy environments. Since the search space for optimization is vast and ill-defined, we develop *genetic* VQS detailing a GA approach to *variationally* and *evolutionarily* optimize PQCs for VQS state preparation in NISQ sensing, e.g., scalar and vector magnetic-field sensing.
- We provide metrologically resourceful ansatzes designed to create genetic VQS probe states that maximize measurement precision in terms of the quantum Fisher information (QFI) under anisotropic quantum noise such as the bit-flip, dephasing (or phase-flip), and amplitude-damping (or energy-relaxation) noise. These tailored VQS probe states exhibit high-sensitivity estimation capacity as quantified by the quantum Cramér–Rao bound (QCRB) under all inherent quantum noise, compared with maximally entangled GHZ or product (separable) states.
- We integrate the QAB protocol into VQS networks to anonymously share sensing information among network sensors—ensuring *anonymity* and *untraceability* of sensing data. This QAS broadcast follows a series

TABLE I
EXPANSIONS OF IMPORTANT ACRONYMS

Acronym	Expansion	Acronym	Expansion
BEP	bit error probability	CNOT	controlled-NOT
CPTP	completely positive trace-preserving	GA	genetic algorithm
GHZ	Greenberger–Horne–Zeilinger	HEA	hardware efficient ansatz
IoT	Internet of Things	ISAC	integrated sensing and communication
NISQ	noisy intermediate-scale quantum	PQC	parameterized quantum circuit
QAB	quantum anonymous broadcast	QAC	quantum anonymous communication
QAS	quantum anonymous sensing	QCRB	quantum Cramér–Rao bound
QFI	quantum Fisher information	QFIM	quantum Fisher information matrix
QSN	quantum sensing network	SQL	standard quantum limit
VQA	variational quantum algorithm	VQS	variational quantum sensing

of steps—i.e., i) broadcast-carrier preparation (GHZ distribution); ii) broadcast modulation (Hadamard and conditional bit-flip operations); iii) broadcast demodulation (computational basis measurement and classical announcement); and iv) broadcast decision (modulo sum calculation).

- We derive the broadcast bit error probability (BEP) for the QAB protocol under anisotropic quantum noise. We show that this QAS broadcast is *error-free*, i.e., zero-BEP under the bit-flip noise, while its BEP under both dephasing and amplitude-damping noises linearly scales with the noise parameter and the number of network sensors in the *low-noise* regime.

The remainder of this paper is organized as follows. Section II introduces quantum sensing and its fundamental limits, Section III briefly reviews the VQAs, and Section IV formally provides the VQS framework. Section V develops the integrated framework of genetic VQS and QAB for QAS networks in noisy environments. Finally, Section VI concludes the paper with a brief summary. In the Appendix, we give the derivations of the BEP for the QAB protocol under bit-flip, dephasing, and amplitude-damping noises. Important acronyms are summarized in Table I.

II. QUANTUM SENSING

A. Quantum Sensing Frameworks

Generally, quantum sensing follows a series of steps: probe preparation, probe interaction, probe measurement, and estimation.

1) *Probe Preparation:* The initial state $|\psi_0\rangle$ of the sensing protocol is evolved by a specific operator to prepare the quantum sensor for interaction with a system of interest using a suitable quantum state. This initial state $|\psi_0\rangle$ is typically set to a known quantum state, such as $|\psi_0\rangle = |0\rangle$. Using an operator $\boldsymbol{W}$, the initial state $|\psi_0\rangle$ is evolved to probe state $|\psi\rangle = \boldsymbol{W}|\psi_0\rangle$ for the sensing purpose.
2) *Probe Interaction:* Sensing is performed by the prepared probe state $|\psi\rangle$ interacting with a system characterized by a Hamiltonian $\boldsymbol{\mathcal{H}}$. Let η be the physical quantity to be sensed. This quantity is encoded in the system by the unitary operation $\boldsymbol{U}(\boldsymbol{\mathcal{H}};\eta)$ acting on the probe state as follows [42]:
$$|\psi(\eta)\rangle = \boldsymbol{U}(\boldsymbol{\mathcal{H}};\eta)|\psi\rangle = \exp(-\imath\boldsymbol{\mathcal{H}}\eta)|\psi\rangle \quad (1)$$
where $\imath = \sqrt{-1}$.
3) *Probe Measurement:* To extract information about the sensing quantity η, the interacted probe state $|\psi(\eta)\rangle$ is measured. Let $\{|\phi_i\rangle\}$ be a nominal measurement basis. This basis is transformed by applying the unitary operator $\boldsymbol{V}$ to get a desired measurement basis $\{\boldsymbol{V}|\phi_i\rangle\}$.
4) *Estimation:* The final step of the protocol involves estimating the unknown quantity η encoded in the evolved state $|\psi(\eta)\rangle$ by measuring it using the measurement basis $\{\boldsymbol{V}|\phi_i\rangle\}$. The estimate of η is then a function $\hat{\eta}(\mu)$ of measurement outcome μ.

Due to the probabilistic nature of quantum measurements, repetitions of sensing are performed to increase the estimation precision. These repeated measurements can be performed in parallel to save the protocol's running time.

B. Quantum Limits

The precision of the estimator $\hat{\eta}$ depends on the sensitivity of the probe state $|\psi\rangle$ on η encoded by the unitary operation $\boldsymbol{U}(\boldsymbol{\mathcal{H}};\eta)$. This sensitivity can be quantified with the QFI, which is a generalization of classical Fisher information to the quantum regime, obtained by maximizing the classical Fisher information over all possible quantum measurement settings. The QFI $J_\eta(\boldsymbol{\rho})$ is defined using a logarithmic derivative operator $\boldsymbol{\Lambda}$ for a quantum state (in general a density matrix) $\boldsymbol{\rho}(\eta)$ as follows [43]:
$$J_\eta(\boldsymbol{\rho}) = \mathrm{tr}\left[\boldsymbol{\Lambda}^2\boldsymbol{\rho}(\eta)\right] \quad (2)$$
where $\mathrm{tr}(\cdot)$ is the trace operator, $\boldsymbol{\Lambda}$ is implicitly defined as
$$\frac{\partial\boldsymbol{\rho}(\eta)}{\partial\eta} = \frac{1}{2}\{\boldsymbol{\Lambda}, \boldsymbol{\rho}(\eta)\}, \quad (3)$$
and $\{\boldsymbol{A}, \boldsymbol{B}\} = \boldsymbol{AB} + \boldsymbol{BA}$ is the anti-commutator. Note that the operator $\boldsymbol{\Lambda}$ is called the symmetric logarithmic derivative due to the non-commuting behavior of operators in the quantum state space.

Let $\mathcal{F}(\boldsymbol{\rho}, \boldsymbol{\sigma})$ be the fidelity between two quantum states $\boldsymbol{\rho}$ and $\boldsymbol{\sigma}$ [44]:
$$\mathcal{F}(\boldsymbol{\rho}, \boldsymbol{\sigma}) = \left(\mathrm{tr}\sqrt{\sqrt{\boldsymbol{\rho}}\boldsymbol{\sigma}\sqrt{\boldsymbol{\rho}}}\right)^2, \quad (4)$$

which simplifies to the pure-state fidelity $\mathcal{F}(|\psi\rangle, |\phi\rangle) = |\langle\psi|\phi\rangle|^2$ when both $\boldsymbol{\rho}$ and $\boldsymbol{\sigma}$ are pure states, i.e., rank-1 projectors onto state vectors $|\psi\rangle$ and $|\phi\rangle$. The sensitivity of the probe state $|\psi\rangle$ with respect to the parameterized evolution state $|\psi(\eta)\rangle$ is related to the fidelity $|\langle\psi|\psi(\eta)\rangle|^2$ as [45]

$$J_\eta(|\psi\rangle) = \lim_{\eta\to 0} 8\left(\frac{1-\sqrt{\mathcal{F}(|\psi\rangle, |\psi(\eta)\rangle)}}{\eta^2}\right) \tag{5}$$

where the QFI depends on the probe state $|\psi\rangle$ with given encoding Hamiltonian. For the parameterized evolution in (1) generated by the Hamiltonian $\boldsymbol{\mathcal{H}}$, the QFI can be expressed by the variance of the Hamiltonian $\boldsymbol{\mathcal{H}}$ as follows [46]:

$$J_\eta(|\psi\rangle) = 4\left(\langle\psi|\boldsymbol{\mathcal{H}}^2|\psi\rangle - \langle\psi|\boldsymbol{\mathcal{H}}|\psi\rangle^2\right). \tag{6}$$

With N-qubit unbiased estimates $\hat{\eta}$, a bound on the precision of estimating η is given by QCRB, i.e., SQL as follows [47]:

$$\mathrm{Var}[\hat{\eta}] \geq \frac{1}{NJ_\eta(|\psi\rangle)} \tag{7}$$

where $\mathrm{Var}[\hat{\eta}]$ is the variance of $\hat{\eta}$.

Quantum metrology aims to beat the SQL by leveraging quantum properties such as entanglement. Let $\lambda_{\max}$ and $\lambda_{\min}$ be the maximum and minimum eigenvalues of the Hamiltonian $\boldsymbol{\mathcal{H}}$, respectively. Expanding the Hamiltonian in its eigenvector basis, from (6) it follows that the QFI is maximized when the measurement outcomes are $\lambda_{\max}$ and $\lambda_{\min}$ with equal probability. Hence, the QFI is maximized when the probe state $|\psi\rangle$ is in an equal superposition of the extreme eigenstates:

$$|\psi\rangle = \frac{|\lambda_{\max}\rangle + |\lambda_{\min}\rangle}{\sqrt{2}}. \tag{8}$$

For N-qubit estimation, the Hamiltonian governing the full system is $\boldsymbol{\mathcal{H}}^{\oplus N}$ where $\oplus$ denotes the Kronecker sum.[1] Hence, the maximum and minimum eigenvalues of this full Hamiltonian are equal to $N\lambda_{\max}$ and $N\lambda_{\min}$ corresponding to the extreme eigenvectors $|\lambda_{\max}\rangle^{\otimes N}$ and $|\lambda_{\min}\rangle^{\otimes N}$, respectively. To maximize the variance of the total Hamiltonian $\boldsymbol{\mathcal{H}}^{\oplus N}$, the N-qubit probe state $|\boldsymbol{\psi}\rangle$ should be prepared as follows [47]:

$$|\boldsymbol{\psi}\rangle = \frac{1}{\sqrt{2}}\left(|\lambda_{\max}\rangle^{\otimes N} + |\lambda_{\min}\rangle^{\otimes N}\right), \tag{9}$$

which is an *entangled* state. Using this entangled state, the estimation precision scales as the Heisenberg limit [47]

$$\mathrm{Var}[\hat{\eta}] \geq \frac{1}{N^2 J_\eta(|\psi\rangle)}. \tag{10}$$

Hence, the SQL can be surpassed by exploiting quantum resources such as entanglement.

C. Multiparameter Sensing

Extension toward multiparameter quantum sensing is not straightforward from a single parameter due to the non-commuting property of quantum operators. This can cause incompatibility among the measurement operators for each parameter. This incompatibility results in an intricate tradeoff to simultaneously extract information from multiple parameters. Let $\boldsymbol{\eta} = (\eta_1, \eta_2, \ldots, \eta_K)$ be a vector of unknown parameters and these K parameters be encoded using the Hamiltonian $\bar{\boldsymbol{\mathcal{H}}} = (\boldsymbol{\mathcal{H}}_1, \boldsymbol{\mathcal{H}}_2, \ldots, \boldsymbol{\mathcal{H}}_K)$ in a unitary operator [48]

$$\boldsymbol{U}(\bar{\boldsymbol{\mathcal{H}}}; \boldsymbol{\eta}) = \exp\left(-\sum_{k=1}^{K} \imath \boldsymbol{\mathcal{H}}_k \eta_k\right) \tag{11}$$

where $\boldsymbol{\mathcal{H}}_k$ is the Hamiltonian that encodes the kth parameter η_k. In a multiparameter case, the (i,j)th element of the QFI matrix (QFIM) $\boldsymbol{J}_{\boldsymbol{\eta}}(\boldsymbol{\rho})$ is defined by [49]

$$[\boldsymbol{J}_{\boldsymbol{\eta}}(\boldsymbol{\rho})]_{ij} = \frac{1}{2}\mathrm{tr}\left(\boldsymbol{\rho}(\boldsymbol{\eta})\{\boldsymbol{\Lambda}_i, \boldsymbol{\Lambda}_j\}\right) \tag{12}$$

where the operator $\boldsymbol{\Lambda}_i$ is the symmetric logarithmic derivative for the parameter η_i, defined as

$$\frac{\partial\boldsymbol{\rho}(\boldsymbol{\eta})}{\partial\eta_i} = \frac{1}{2}\{\boldsymbol{\Lambda}_i, \boldsymbol{\rho}(\boldsymbol{\eta})\}. \tag{13}$$

For the probe state $|\psi\rangle$, the (i,j)th element of the QFIM $\boldsymbol{J}_{\boldsymbol{\eta}}(|\psi\rangle)$ is given by [49]

$$[\boldsymbol{J}_{\boldsymbol{\eta}}(|\psi\rangle)]_{ij} = 2\langle\psi|\{\boldsymbol{\mathcal{H}}_i, \boldsymbol{\mathcal{H}}_j\}|\psi\rangle - 4\langle\psi|\boldsymbol{\mathcal{H}}_i|\psi\rangle\langle\psi|\boldsymbol{\mathcal{H}}_j|\psi\rangle, \tag{14}$$

which again depends on the probe state $|\psi\rangle$ with given encoding Hamiltonian. The QFIM relates to the fidelity as follows [50]:

$$\boldsymbol{\eta}\boldsymbol{J}_{\boldsymbol{\eta}}(|\psi\rangle)\boldsymbol{\eta}^T \approx 8\|\boldsymbol{\eta}\|^2\left(\frac{1-\sqrt{\mathcal{F}(|\psi\rangle, |\psi(\epsilon\boldsymbol{\eta}/\|\boldsymbol{\eta}\|)\rangle)}}{\epsilon^2}\right) \tag{15}$$

where T is the transpose operator and $\epsilon \ll 1$ is an arbitrary small number. Using the QFIM, the sum of the individual variance for the estimator $\hat{\eta}_k$ is lower bounded by [51]

$$\sum_{k=1}^{K}\mathrm{Var}[\hat{\eta}_k] \geq \mathrm{tr}\left[\boldsymbol{J}_{\boldsymbol{\eta}}^{-1}(|\psi\rangle)\right]. \tag{16}$$

III. Variational Quantum Algorithms

VQAs have emerged as potential solutions for tackling a range of problems using currently available quantum devices. The VQAs are iterative algorithms that combine quantum and classical computing to find a high-quality solution for a problem of interest. Quantum computing is used to produce a trial solution, while classical computing is used to guide the quantum computer to generate a better solution. Generally, the VQAs consist of three main components, namely, the PQC, cost function, and classical optimizer.

A. Parameterized Quantum Circuits

A PQC, often called a variational quantum circuit or ansatz, is a distinct class of quantum circuits with adjustable parameters to be tuned using an optimization algorithm by means of a cost function. The design of PQCs can be inspired by insights from a problem of interest. In the case where there is a lack of information about the problem at hand, the PQC architecture is designed to be general-purpose.

[1]For two matrices (operators) $\boldsymbol{A}$ and $\boldsymbol{B}$ of dimensions $m\times m$ and $n\times n$, the Kronecker sum is defined as $\boldsymbol{A}\oplus\boldsymbol{B} = \boldsymbol{A}\otimes\boldsymbol{I}_n + \boldsymbol{I}_m\otimes\boldsymbol{B}$, where $\otimes$ denotes the tensor product and $\boldsymbol{I}_n$ is the $n\times n$ identity operator. Here, $\boldsymbol{I}_2$ is denoted by $\boldsymbol{I}$ for the qubit case.

The PQC generally consists of a series of L unitary operations as follows [52]:

$$\boldsymbol{U}\left(\bar{\boldsymbol{\mathcal{Q}}};\boldsymbol{\theta}\right)=\boldsymbol{U}\left(\boldsymbol{\mathcal{Q}}_L;\theta_L\right)\cdots\boldsymbol{U}\left(\boldsymbol{\mathcal{Q}}_2;\theta_2\right)\boldsymbol{U}\left(\boldsymbol{\mathcal{Q}}_1;\theta_1\right) \quad (17)$$

where $\boldsymbol{\theta}=(\theta_1,\theta_2,\ldots,\theta_L)$ is the parameter vector to be optimized, $\bar{\boldsymbol{\mathcal{Q}}}=(\boldsymbol{\mathcal{Q}}_1,\boldsymbol{\mathcal{Q}}_2,\ldots,\boldsymbol{\mathcal{Q}}_L)$, and $\boldsymbol{\mathcal{Q}}_\ell$ is the Hamiltonian that encodes the ℓth parameter θ_ℓ for the PQC. Typically, $\boldsymbol{U}\left(\boldsymbol{\mathcal{Q}}_\ell;\theta_\ell\right)$ is local unitary or controlled unitary. The controlled unitary operators introduce entanglement within the system. On top of controlled operators, unitary operators with interacting Hamiltonians can also produce entanglement. The PQC is required to be able to generate a diverse set of quantum states in order to explore various potential solutions. Furthermore, this quantum circuit needs to provide sufficient entanglement generation and manipulation capability to produce more intricate entanglement within the system [33].

B. Cost Functions

The quality of a trial solution generated by PQC using trainable parameters $\boldsymbol{\theta}$ is evaluated through a cost function. Typically, the cost function can be written in the form of [33]

$$C\left(\boldsymbol{\theta}\right)=f\left(\left\{\left|\phi_i\right\rangle\right\},\left|\psi\left(\boldsymbol{\theta}\right)\right\rangle\right) \quad (18)$$

where f is a real-valued function and $\left|\psi\left(\boldsymbol{\theta}\right)\right\rangle$ is the trial state generated by the PQC. This cost function is highly reliant on the problem at hand and needs to be trainable by a classical computer. Minimizing the cost function corresponds to optimizing the trial solution. As the number of parameters increases, the landscape of the cost function becomes more complicated requiring a good classical optimizer to find a high-quality solution [33].

C. Classical Optimizers

The main task for the classical optimizer is to navigate the landscape of the cost function to avoid local minima and converge to global optima by tuning the trainable parameters $\boldsymbol{\theta}$, making it a core component for VQAs. The optimizer seeks to find the optimal parameter

$$\boldsymbol{\theta}_\star=\arg\min\, C\left(\boldsymbol{\theta}\right) \quad (19)$$

by minimizing the cost function over the trainable parameters. As the number of parameters increases, the number of local minima can also increase, leading to the optimizer being trapped at this local minima [53]. The ability of the optimizer to avoid these local traps is crucial for finding a good potential solution for the problem at hand.

A gradient-based or -free optimizer can be used to train the parameters of VQAs. The gradient method guides the optimizer to update the parameter in the direction of minimizing the cost function. Typically, in VQAs, the gradient is obtained by the parameter-shift rule that amounts to computing the partial derivatives $\partial C/\partial\theta_i$ [54]. The common gradient methods used in VQAs are stochastic gradient descent and Adam optimizer [55], [56]. The gradient optimizer is prone to be trapped at local minima and in regions where the gradient of the cost function is flat, thus hindering its ability to find the global minima [57]. Gradient-free optimizers are used to tackle this issue, such as the constrained optimization by linear approximations (COBYLA), Broyden-Fletcher-Goldfarb-Shanno (BFGS), and evolutionary algorithms [58], [59].

IV. Variational Quantum Sensing

In line with VQAs, the VQS begins by choosing a PQC. The chosen PQC is designed to adaptively learn the optimal settings for both the probe preparation and measurement operators.

A. Single-Parameter Sensing

Note from (9) that the optimal probe state is in the entangled form of an equal superposition of two orthogonal states, where all subsystems for each state are in the same exact state.

1) Probe Preparation: The VQS protocol starts with N qubits all initialized to $|0\rangle$, i.e., the N-qubit state $|0\rangle^{\otimes N}$. Let $\boldsymbol{H}=\left(\boldsymbol{\sigma}_{\mathrm{x}}+\boldsymbol{\sigma}_{\mathrm{z}}\right)/\sqrt{2}$ be the Hadamard operator where $\boldsymbol{\sigma}_{\mathrm{x}}=|0\rangle\langle1|+|1\rangle\langle0|$ and $\boldsymbol{\sigma}_{\mathrm{z}}=|0\rangle\langle0|-|1\rangle\langle1|$ are the Pauli-x and -z operators, respectively. Then, by applying the Hadamard gate $\boldsymbol{H}$ to the first qubit and then sequentially performing controlled-NOT (CNOT) or controlled-$\boldsymbol{\sigma}_{\mathrm{x}}$ gates between the first qubit (control) and all successive qubits (target), the initial state $|\psi_0\rangle$ of the N-qubit sensing system is prepared in the N-partite (maximally entangled) GHZ state as follows:

$$\left|\psi_0\right\rangle=\boldsymbol{G}_N\cdots\boldsymbol{G}_2\boldsymbol{G}_1\left|0\right\rangle^{\otimes N}=\frac{1}{\sqrt{2}}\left(\left|0\right\rangle^{\otimes N}+\left|1\right\rangle^{\otimes N}\right) \quad (20)$$

where

$$\boldsymbol{G}_1=\boldsymbol{H}\otimes\boldsymbol{I}^{\otimes(N-1)} \quad (21)$$

$$\boldsymbol{G}_i=|0\rangle\langle0|\otimes\boldsymbol{I}^{\otimes(N-1)}+|1\rangle\langle1|\otimes\tilde{\boldsymbol{X}}_{i,N} \quad (22)$$

with the Pauli operator $\boldsymbol{\sigma}_{\mathrm{x}}$ acting on the ith qubit

$$\tilde{\boldsymbol{X}}_{i,N}=\boldsymbol{I}^{\otimes(i-2)}\otimes\boldsymbol{\sigma}_{\mathrm{x}}\otimes\boldsymbol{I}^{\otimes(N-i)} \quad (23)$$

for $i=2,3,\ldots,N$. After preparing the initial GHZ state $|\psi_0\rangle$, a unitary preparation operator for the basis change can be parameterized such as $\boldsymbol{W}_{\boldsymbol{\theta}}=\boldsymbol{U}\left(\bar{\boldsymbol{\mathcal{Q}}};\boldsymbol{\theta}\right)$ to obtain the trial probe state $\left|\psi\left(\boldsymbol{\theta}\right)\right\rangle=\boldsymbol{W}_{\boldsymbol{\theta}}\left|\psi_0\right\rangle$, where $\boldsymbol{\theta}$ are the parameters to be optimized for probe state preparation. Since the entanglement structure of the optimal probe state is embedded in the initial state $|\psi_0\rangle$, the PQC for the preparation operator $\boldsymbol{W}_{\boldsymbol{\theta}}$ can be designed by local parameterized unitary operations only.

2) Probe Interaction: The trial probe state $\left|\psi\left(\boldsymbol{\theta}\right)\right\rangle$ interacts with the unknown parameter η through the unitary operation $\boldsymbol{U}\left(\boldsymbol{\mathcal{H}}^{\oplus N};\eta\right)$ to create the state

$$\left|\psi\left(\boldsymbol{\theta};\eta\right)\right\rangle=\boldsymbol{U}\left(\boldsymbol{\mathcal{H}}^{\oplus N};\eta\right)\left|\psi\left(\boldsymbol{\theta}\right)\right\rangle. \quad (24)$$

This interaction state is then measured by the measurement operator. Based on the measurement outcomes, the parameter vector $\boldsymbol{\theta}$ is updated to minimize a cost function $C\left(\boldsymbol{\theta};\eta\right)$. Note that the cost function $C\left(\boldsymbol{\theta};\eta\right)$ quantifies how well the trial probe state $\left|\psi\left(\boldsymbol{\theta}\right)\right\rangle$ estimates the unknown parameter η using the QFI in (5). To maximize the QFI, we utilize the fidelity as the cost function as follows:

$$C\left(\boldsymbol{\theta};\eta\right)=\left|\left\langle\psi\left(\boldsymbol{\theta}\right)\left|\psi\left(\boldsymbol{\theta};\eta\right)\right\rangle\right|^2. \quad (25)$$

Hence, we need to compute the probability of the interaction state $|\psi(\boldsymbol{\theta};\eta)\rangle$ collapses to the trial probe state $|\psi(\boldsymbol{\theta})\rangle$ for learning the PQC.

3) Probe Measurement: Since the VQS system is initialized in the computational basis and assuming the measurement is also performed in computational basis, the unitary operator $\boldsymbol{V}_{\boldsymbol{\theta}}$ for the change of measurement basis can be obtained by the inverse operation of preparing the trial probe state $|\psi(\boldsymbol{\theta})\rangle$ from the state $|0\rangle^{\otimes N}$ as follows:

$$\boldsymbol{V}_{\boldsymbol{\theta}}^{\dagger} = \boldsymbol{W}_{\boldsymbol{\theta}}\boldsymbol{G}_N \cdots \boldsymbol{G}_2\boldsymbol{G}_1 \tag{26}$$

where $\dagger$ denotes the conjugate transpose. Now, the cost function can be written as

$$C(\boldsymbol{\theta};\eta) = \left|\langle 0|^{\otimes N} |\boldsymbol{\zeta}(\boldsymbol{\theta};\eta)\rangle\right|^2 \tag{27}$$

where

$$|\boldsymbol{\zeta}(\boldsymbol{\theta};\eta)\rangle = \boldsymbol{V}_{\boldsymbol{\theta}}\boldsymbol{U}\left(\boldsymbol{\mathcal{H}}^{\oplus N};\eta\right)\boldsymbol{V}_{\boldsymbol{\theta}}^{\dagger}|0\rangle^{\otimes N} \tag{28}$$

is the PQC output state ready for the computational basis measurement. Hence, the cost function $C(\boldsymbol{\theta};\eta)$ can be seen as the probability such that the output state $|\boldsymbol{\zeta}(\boldsymbol{\theta};\eta)\rangle$ would collapses into the state $|0\rangle^{\otimes N}$.

B. Multiparameter Sensing

In a single-parameter case, the structure of the optimal probe state is analytically known, which guides the design of PQCs. The optimal structure is generally challenging to obtain in a multiparameter case. Hence, a more generic PQC is designed to explore a large range of trial solutions.

1) Probe Preparation: To devise a more generic PQC, consider an entangling unitary operator $\boldsymbol{U}(\boldsymbol{\mathcal{Q}}_\ell;\theta_\ell)$ which can be written in the form

$$\boldsymbol{U}(\boldsymbol{\mathcal{Q}}_\ell;\theta_\ell) = |0\rangle\langle 0| \otimes \boldsymbol{I} + |1\rangle\langle 1| \otimes \exp(-\imath\boldsymbol{\mathcal{Q}}_\ell\theta_\ell). \tag{29}$$

This is a controlled unitary operator that only performs the local unitary operation $\exp(-\imath\boldsymbol{\mathcal{Q}}_\ell\theta_\ell)$ to the target qubit when the control qubit is in state $|1\rangle$ and leaves it unchanged, otherwise. Using interaction Hamiltonian $\boldsymbol{\mathcal{Q}}_\ell$, another entangling unitary operator is in the form

$$\boldsymbol{U}(\boldsymbol{\mathcal{Q}}_\ell;\theta_\ell) = \exp(-\imath\boldsymbol{\mathcal{Q}}_\ell\theta_\ell). \tag{30}$$

Let the initial state of the quantum sensor be $|\psi_0\rangle = |0\rangle^{\otimes N}$. Then, the trial probe state is prepared as follows:

$$|\psi(\boldsymbol{\theta})\rangle = \boldsymbol{U}\left(\bar{\boldsymbol{\mathcal{Q}}};\boldsymbol{\theta}\right)|0\rangle^{\otimes N}. \tag{31}$$

2) Probe Interaction: The unknown parameters $\boldsymbol{\eta}$ are encoded by the total Hamiltonian

$$\bar{\boldsymbol{\mathcal{H}}}^{\oplus N} = \left(\boldsymbol{\mathcal{H}}_1^{\oplus N}, \boldsymbol{\mathcal{H}}_2^{\oplus N}, \ldots, \boldsymbol{\mathcal{H}}_K^{\oplus N}\right) \tag{32}$$

in the unitary operator $\boldsymbol{U}\left(\bar{\boldsymbol{\mathcal{H}}}^{\oplus N};\boldsymbol{\eta}\right)$, which then interacts with the trial probe state $|\psi(\boldsymbol{\theta})\rangle$ to generate the state

$$|\psi(\boldsymbol{\theta};\boldsymbol{\eta})\rangle = \boldsymbol{U}\left(\bar{\boldsymbol{\mathcal{H}}}^{\oplus N};\boldsymbol{\eta}\right)\boldsymbol{U}\left(\bar{\boldsymbol{\mathcal{Q}}};\boldsymbol{\theta}\right)|0\rangle^{\otimes N}. \tag{33}$$

This multiparameter evolved state is evaluated by the cost function $C(\boldsymbol{\theta};\boldsymbol{\eta})$ using the quantum measurement outcomes. Following (15), we also use the fidelity between the trial probe state $|\psi(\boldsymbol{\theta})\rangle$ and the generated state $|\psi(\boldsymbol{\theta};\boldsymbol{\eta})\rangle$ as the cost function.

3) Probe Measurement: Since the cost function is the fidelity between the trial probe and generated states, the unitary operator $\boldsymbol{V}_{\boldsymbol{\theta}}$ for the change of measurement basis is simply given by

$$\boldsymbol{V}_{\boldsymbol{\theta}} = \boldsymbol{U}^{\dagger}\left(\bar{\boldsymbol{\mathcal{Q}}};\boldsymbol{\theta}\right). \tag{34}$$

The cost function is then calculated by evolving the generated state $|\psi(\boldsymbol{\theta};\boldsymbol{\eta})\rangle$ using $\boldsymbol{U}\left(\bar{\boldsymbol{\mathcal{Q}}};\boldsymbol{\theta}\right)$ and then computing the probability of finding the state $|0\rangle^{\otimes N}$ as follows:

$$C(\boldsymbol{\theta};\boldsymbol{\eta}) = \left|\langle 0|^{\otimes N}\boldsymbol{U}^{\dagger}\left(\bar{\boldsymbol{\mathcal{Q}}};\boldsymbol{\theta}\right)|\psi(\boldsymbol{\theta};\boldsymbol{\eta})\rangle\right|^2. \tag{35}$$

V. Integrated VQS With QAC

Consider a QSN of M sensors where each quantum sensor can tailor its quantum state variationally. These sensors employ a *genetic* VQA to variationally prepare the probe state. The PQC is designed by a GA approach for the physical quantity of interest (e.g., magnetic-field sensing for localization or classification). After interacting and estimating the physical quantity, the sensor anonymously broadcasts the sensing information to all network sensors. This framework for QAS networks integrates the genetic VQS with the QAB protocol to ensure anonymity and untraceability.

A. Genetic VQS

Finding a high-quality PQC is difficult due to the large PQC space [33]. GAs leverage a population-based method where multiple potential solutions are evaluated simultaneously to enhance the algorithms' ability to converge to a high-quality solution. Thus, a genetic approach inspired by the process of natural selection is utilized to heuristically search the PQC structure for the magnetic-field sensing task.

1) Genetic PQCs: PQCs used in quantum algorithms determine the quality of a probe state obtained by VQS. A GA method is employed to find the PQC structure [60]. The GA begins by initializing the population that consists of q chromosomes

$$\mathcal{P} = \left\{\mathfrak{p}_1, \mathfrak{p}_2, \ldots, \mathfrak{p}_q\right\}. \tag{36}$$

The ith chromosome $\mathfrak{p}_i$ contains a series of genes as follows:

$$\mathfrak{p}_i = \begin{bmatrix} (\boldsymbol{\mathcal{A}}_{i1}, |c_{i1}\rangle, |t_{i1}\rangle, \theta_{i1}) \\ (\boldsymbol{\mathcal{A}}_{i2}, |c_{i2}\rangle, |t_{i2}\rangle, \theta_{i2}) \\ \vdots \\ (\boldsymbol{\mathcal{A}}_{i\ell_i}, |c_{i\ell_i}\rangle, |t_{i\ell_i}\rangle, \theta_{i\ell_i}) \end{bmatrix} \tag{37}$$

where $\boldsymbol{\mathcal{A}}_{ij}$ is a Hamiltonian taken from a set $\{\boldsymbol{\sigma}_{\mathrm{x}}, \boldsymbol{\sigma}_{\mathrm{y}}, \boldsymbol{\sigma}_{\mathrm{z}}\}$ of Pauli operators, $\boldsymbol{\sigma}_{\mathrm{y}} = \imath\boldsymbol{\sigma}_{\mathrm{x}}\boldsymbol{\sigma}_{\mathrm{z}}$ is the Pauli-y operator, $|c_{ij}\rangle$ is the control qubit, $|t_{ij}\rangle$ is the target qubit, θ_{ij} is the parameter, and ℓ_i is the length of genes. The gene is mapped into a single- or two-qubit unitary operator. For a single-qubit unitary operator, the control qubit $|c_{ij}\rangle$ is not defined, and the unitary operator $\boldsymbol{U}(\boldsymbol{\mathcal{A}}_{ij};\theta_{ij}) = \exp(-\imath\boldsymbol{\mathcal{A}}_{ij}\theta_{ij})$ is applied to the target qubit $|t_{ij}\rangle$. The two-qubit unitary operator is in the controlled unitary form $\boldsymbol{U}(\boldsymbol{\mathcal{A}}_{ij};\theta_{ij}) = |0\rangle\langle 0| \otimes \boldsymbol{I} + |1\rangle\langle 1| \otimes \exp(-\imath\boldsymbol{\mathcal{A}}_{ij}\theta_{ij})$ and is applied to the control and target qubits $|c_{ij}\rangle \otimes |t_{ij}\rangle$.

All the chromosomes in the population are evaluated by calculating the QFI for the generated state

$$|\psi(\boldsymbol{\theta})\rangle = \mathcal{M}\left(\mathfrak{g}_{\ell_i}\right)\cdots\mathcal{M}\left(\mathfrak{g}_2\right)\mathcal{M}\left(\mathfrak{g}_1\right)|\psi_0\rangle \tag{38}$$

where $\mathcal{M}$ is the map from the gene to the unitary operator, $\mathfrak{g}_k$ is the kth gene of the chromosome, and $|\psi_0\rangle = |0\rangle^{\otimes N}$. The density matrix $|\psi(\boldsymbol{\theta})\rangle\langle\psi(\boldsymbol{\theta})|$ is evolved using the Lindblad master equation. Based on the corresponding QFI, each chromosome with the best fitness is chosen as a parent for generating the next generation of the population. In addition to the best chromosome, the other parents are determined by using tournament selection, where the tournament round and size are set to r and s. This makes the total parent chromosomes of $r+1$. These parents are included in the next generation. To generate the offspring, the crossover operation that takes two parents as the input and generates a new chromosome is employed. The crossover operation extracts a sequence of genes with random length from one parent and it becomes the basis for the child genes. Then, another sequence of genes with random length from a different parent is appended to the child's chromosome. After the child is generated from the crossover operation, the child undergoes a series of mutation operations.

- *Qubit mutation operator*: randomly changes the control and target qubits of each gene at a specific mutation probability.
- *Parameter mutation operator*: adds the parameter of each gene with a value taken from a zero-mean normal distribution with a chosen standard deviation at a specific mutation probability.
- *Genes deletion operator*: randomly removes a series of genes within the chromosome.
- *Genes insertion operator*: generates a random series of genes which are then inserted randomly in the chromosome.
- *Genes replacement operator*: sequentially performs gene deletion and insertion operators.
- *Genes swaping operator*: randomly picks two series of genes and swaps them.
- *Genes permutation operator*: randomly selects a series of genes randomly and then randomly shuffles the elements of the series.

The next generation of the population then repeats the same procedures for the evaluation, parent selection, crossover operation, and mutation operation with a specific number of iterations.

2) Scalar Magnetic-Field Sensing: For the single-parameter VQS to estimate the amplitude of a magnetic field, consider that the vector $\boldsymbol{\eta} = (\eta_1, \eta_2, \eta_3)$ of magnetic field components is encoded by the Hamiltonian $\bar{\mathcal{H}} = \frac{1}{2}(\boldsymbol{\sigma}_{\mathrm{x}}, \boldsymbol{\sigma}_{\mathrm{y}}, \boldsymbol{\sigma}_{\mathrm{z}})$ in the unitary operator

$$\boldsymbol{U}\left(\bar{\mathcal{H}}; \boldsymbol{\eta}\right) = \exp\left[-\frac{\imath}{2}\left(\boldsymbol{\sigma}_{\mathrm{x}}\eta_1 + \boldsymbol{\sigma}_{\mathrm{y}}\eta_2 + \boldsymbol{\sigma}_{\mathrm{z}}\eta_3\right)\right]. \tag{39}$$

To cast it as a single-parameter problem, rewrite the Hamiltonian of $\boldsymbol{U}\left(\bar{\mathcal{H}}; \boldsymbol{\eta}\right)$ as $\boldsymbol{\mathcal{H}} = \left(\boldsymbol{\sigma}_{\mathrm{x}}\eta_1 + \boldsymbol{\sigma}_{\mathrm{y}}\eta_2 + \boldsymbol{\sigma}_{\mathrm{z}}\eta_3\right)/\left(2\|\boldsymbol{\eta}\|\right)$ and the unitary evolution as $\boldsymbol{U}\left(\boldsymbol{\mathcal{H}}; \|\boldsymbol{\eta}\|\right) = \exp\left(-\imath\boldsymbol{\mathcal{H}}\|\boldsymbol{\eta}\|\right)$ for VQS to sense the amplitude of the magnetic field $\|\boldsymbol{\eta}\|$.

The eigenvectors of the Hamiltonian $\boldsymbol{\mathcal{H}}$ can be identified by the density matrix form as follows:

$$\boldsymbol{\rho}_\lambda = |\lambda\rangle\langle\lambda| = \frac{1}{2}\left(\boldsymbol{I} + a_1\boldsymbol{\sigma}_{\mathrm{x}} + a_2\boldsymbol{\sigma}_{\mathrm{y}} + a_3\boldsymbol{\sigma}_{\mathrm{z}}\right) \tag{40}$$

where $\boldsymbol{a} = (a_1, a_2, a_3) = \boldsymbol{\eta}/\|\boldsymbol{\eta}\|$ for $|\lambda_{\max}\rangle$ and $\boldsymbol{a} = -\boldsymbol{\eta}/\|\boldsymbol{\eta}\|$ for $|\lambda_{\min}\rangle$. Hence, in the noiseless case, the optimal probe state for the N-qubit sensing system can be obtained variationally with a simple local PQC such as $\boldsymbol{U}\left(\bar{\boldsymbol{\mathcal{Q}}}; \boldsymbol{\theta}\right) = \boldsymbol{U}\left(\boldsymbol{\sigma}_{\mathrm{x}}^{\oplus N}; \boldsymbol{\theta}\right)$ with the initial GHZ state $|\psi_0\rangle$ in (20) to achieve the Heisenberg scaling. In noisy cases, the GHZ-type state may not be optimal due to its sensitivity to noise. For example, when the magnetic field is only in the z-axis direction, i.e., $\boldsymbol{\eta} = (0, 0, \eta_3)$, the GHZ-type and product states have the same precision scaling under dephasing noise. Hence, it is necessary to obtain a better probe state [35]. Consider the completely positive trace-preserving (CPTP) [61] evolution of a quantum state in a noisy environment to be governed by the Lindblad master equation [62]

$$\frac{d\boldsymbol{\rho}_\lambda(t)}{dt} = -\imath\left[\boldsymbol{\mathcal{H}}\|\boldsymbol{\eta}\|, \boldsymbol{\rho}_\lambda(t)\right] + \boldsymbol{\mathcal{L}}\left(\boldsymbol{\rho}_\lambda(t)\right) \tag{41}$$

$$\boldsymbol{\mathcal{L}}\left(\boldsymbol{\rho}_\lambda(t)\right) = \sum_{i=1}^{N}\gamma_i\left(\boldsymbol{\Gamma}_i\boldsymbol{\rho}_\lambda(t)\boldsymbol{\Gamma}_i^\dagger - \frac{1}{2}\left\{\boldsymbol{\Gamma}_i^\dagger\boldsymbol{\Gamma}_i, \boldsymbol{\rho}_\lambda(t)\right\}\right) \tag{42}$$

where $[\boldsymbol{A}, \boldsymbol{B}] = \boldsymbol{AB} - \boldsymbol{BA}$ is the commutator, γ_i is the decay rate, and $\boldsymbol{\Gamma}_i$ is the decay operator. The first term in the master equation (41) corresponds to the noiseless evolution, whereas the second term $\boldsymbol{\mathcal{L}}\left(\boldsymbol{\rho}_\lambda(t)\right)$ relates to the interaction between the system and environment, generating non-unitary dynamics.

1. Bit-Flip Quantum Noise: The decay operator $\boldsymbol{\Gamma}_i$ is given by the bit-flip Pauli operator $\boldsymbol{\sigma}_{\mathrm{x}}$ acting on the ith qubit, i.e., $\boldsymbol{\Gamma}_i = \boldsymbol{X}_{i,N}$ where [63]

$$\boldsymbol{X}_{i,N} = \boldsymbol{I}^{\otimes(i-1)} \otimes \boldsymbol{\sigma}_{\mathrm{x}} \otimes \boldsymbol{I}^{\otimes(N-i)}. \tag{43}$$

Hence, the non-unitary dynamics $\boldsymbol{\mathcal{L}}\left(\boldsymbol{\rho}_\lambda(t)\right)$ for the bit-flip noise is given by

$$\boldsymbol{\mathcal{L}}\left(\boldsymbol{\rho}_\lambda(t)\right) = \sum_{i=1}^{N}\gamma_i\left(\boldsymbol{X}_{i,N}\boldsymbol{\rho}_\lambda(t)\boldsymbol{X}_{i,N} - \boldsymbol{\rho}_\lambda(t)\right). \tag{44}$$

2. Dephasing (Phase-Flip) Quantum Noise: The decay operator $\boldsymbol{\Gamma}_i$ is given by the phase-flip Pauli operator $\boldsymbol{\sigma}_{\mathrm{z}}$ acting on the ith qubit, i.e., $\boldsymbol{\Gamma}_i = \boldsymbol{Z}_{i,N}$ where [63]

$$\boldsymbol{Z}_{i,N} = \boldsymbol{I}^{\otimes(i-1)} \otimes \boldsymbol{\sigma}_{\mathrm{z}} \otimes \boldsymbol{I}^{\otimes(N-i)}. \tag{45}$$

The non-unitary dynamics $\boldsymbol{\mathcal{L}}\left(\boldsymbol{\rho}_\lambda(t)\right)$ for the dephasing noise is then given by

$$\boldsymbol{\mathcal{L}}\left(\boldsymbol{\rho}_\lambda(t)\right) = \sum_{i=1}^{N}\gamma_i\left(\boldsymbol{Z}_{i,N}\boldsymbol{\rho}_\lambda(t)\boldsymbol{Z}_{i,N} - \boldsymbol{\rho}_\lambda(t)\right). \tag{46}$$

3. Amplitude-Damping (Energy-Relaxation) Quantum Noise: The decay operator $\boldsymbol{\Gamma}_i$ is given by the combined Pauli operator $\boldsymbol{\sigma}_{\mathrm{xy}} = \left(\boldsymbol{\sigma}_{\mathrm{x}} + \imath\boldsymbol{\sigma}_{\mathrm{y}}\right)/2$ acting on the ith qubit as follows [64]:

$$\boldsymbol{\Gamma}_i = \boldsymbol{I}^{\otimes(i-1)} \otimes \boldsymbol{\sigma}_{\mathrm{xy}} \otimes \boldsymbol{I}^{\otimes(N-i)}. \tag{47}$$

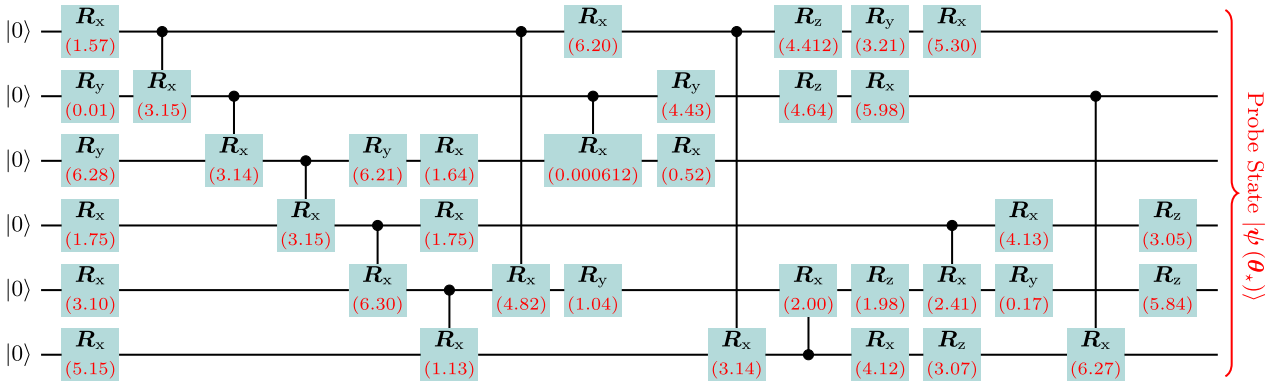

(a) Optimized PQC

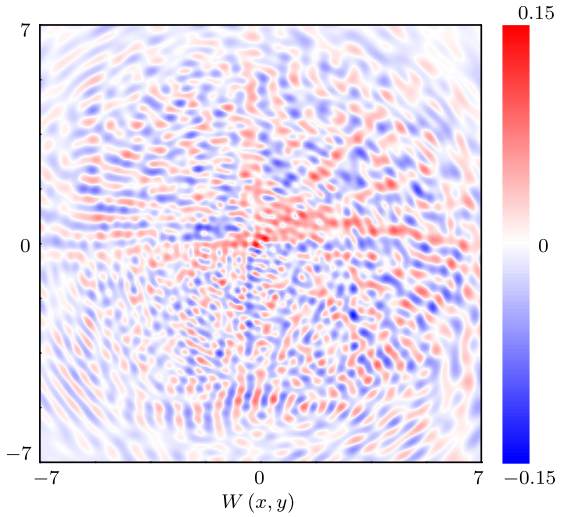

(b) Wigner function

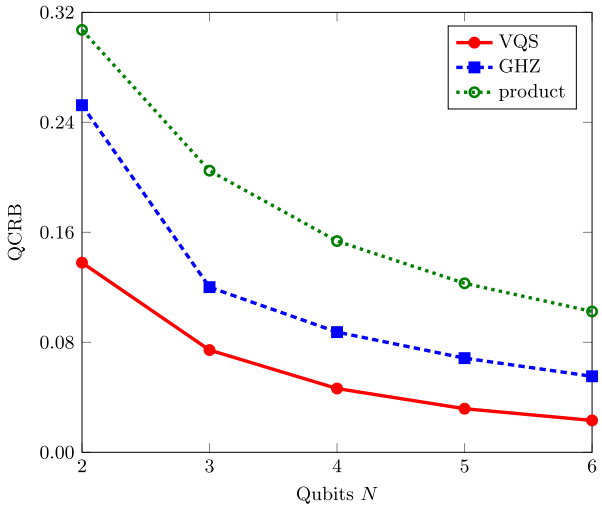

(c) QCRB

Fig. 2. Genetic VQS probe state $|\boldsymbol{\psi}(\boldsymbol{\theta}_\star)\rangle$ for scalar magnetic-field sensing ($N = 6$) under bit-flip noise where the bit-flip noise acts independently on each qubit at the decay rate of $\gamma_i = 0.1$ for all qubits. (a) The PQC structure that maximizes the QFI is obtained by the GA for $N = 6$ where the red values denote the optimized angle parameters. The PQC consists of single-qubit rotation gates $\boldsymbol{R}_{\mathrm{v}}(\theta) = \exp(-\imath\boldsymbol{\sigma}_{\mathrm{v}}\theta/2)$ and two-qubit gates in the form of controlled-$\boldsymbol{R}_{\mathrm{x}}(\theta)$ gates, where $\mathrm{v} \in \{\mathrm{x}, \mathrm{y}, \mathrm{z}\}$ and $\theta \in [0, 2\pi]$. (b) The Wigner function $W(x, y)$ for the optimized VQS probe state $|\boldsymbol{\psi}(\boldsymbol{\theta}_\star)\rangle$ is plotted as a function of phase-space parameters (x, y) using the QuTiP (quantum toolbox in Python) package. (c) The QCRB is plotted for VQS, GHZ, and product states as a function of the number N of qubits involved in the sensing process, where the noisy quantum-state evolution governed by the Lindblad master equation in (41) is also simulated using the QuTiP and the VQS probe state is optimized for each N.

Numerical Examples: Figs. 2–4 show the prepared genetic VQS probe states $|\boldsymbol{\psi}(\boldsymbol{\theta}_\star)\rangle$ for scalar magnetic-field sensing when $N = 6$ under bit-flip, dephasing, and amplitude-damping noises, respectively, where the noise acts independently on each qubit at the decay rate of $\gamma_i = 0.1$ for all qubits. The PQC structure that maximizes the QFI is obtained by the GA with 30 chromosomes ($q = 30$), 3 tournament rounds ($r = 3$), and 7 tournament sizes ($s = 7$) for each N. The PQC consists of single-qubit rotation gates $\boldsymbol{R}_{\mathrm{v}}(\theta) = \exp(-\imath\boldsymbol{\sigma}_{\mathrm{v}}\theta/2)$ and two-qubit controlled-$\boldsymbol{R}_{\mathrm{x}}(\theta)$ gates, where $\mathrm{v} \in \{\mathrm{x}, \mathrm{y}, \mathrm{z}\}$ and $\theta \in [0, 2\pi]$. The optimized angle parameters are shown in red values. The Wigner function $W(x, y)$ for the optimized VQS probe state $|\boldsymbol{\psi}(\boldsymbol{\theta}_\star)\rangle$ is plotted as a function of phase-space parameters (x, y). The Wigner function is a quasi-probability distribution function on the position and momentum variables and is defined for $\boldsymbol{\rho}$ as

$$W(x, y) = \frac{1}{\pi\hbar}\int_{-\infty}^{\infty} \langle x - \tau|\,\boldsymbol{\rho}\,|x + \tau\rangle\, e^{2\imath y\tau/\hbar} d\tau \qquad (48)$$

where $\hbar$ is the reduced Planck's constant. The negative values of the Wigner function indicate the non-classical nature of quantum states [65]. Hence, the Wigner function shows that the tailored VQS probe states $|\boldsymbol{\psi}(\boldsymbol{\theta}_\star)\rangle$ are non-classical as indicated by their negative values. We also compare the QCRB for VQS, GHZ, and product states when $N = 2, 3, 4, 5$, and 6, where the noisy quantum-state evolution governed by the Lindblad master equation in (41). As can be seen in Figs. 2–4, VQS probe states exhibit improved precision bounds for all three types of quantum noise. Both GHZ and product states are in the eigenbasis of the Hamiltonian $\boldsymbol{\mathcal{H}}$. The GHZ and product states are shown to be more prone to the bit-flip and dephasing noises as compared to the amplitude-damping noise. However, the product state is more robust to the dephasing noise than the bit-flip noise and outperforms the GHZ for the amplitude-damping case. The VQS state is also more prone to the bit-flip and dephasing noises than the amplitude-damping noise when $N = 2, 3$, and 4. The VQS state is tailored to have roughly similar precision bounds for all three noises.

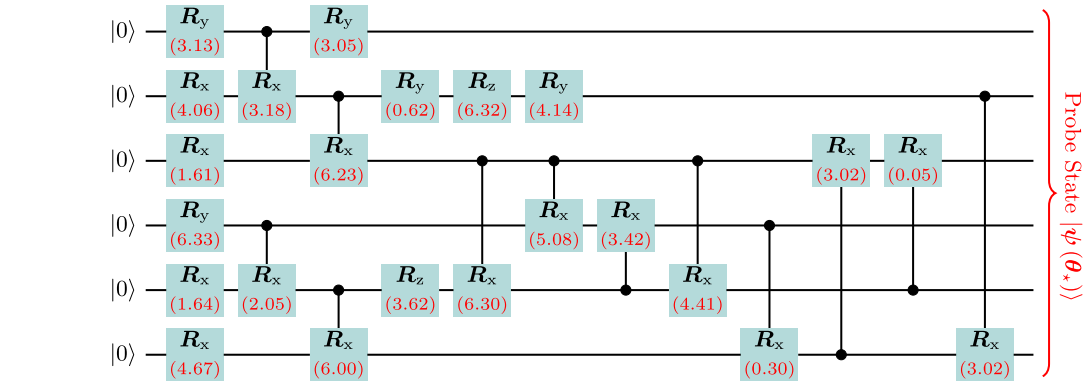

(a) Optimized PQC

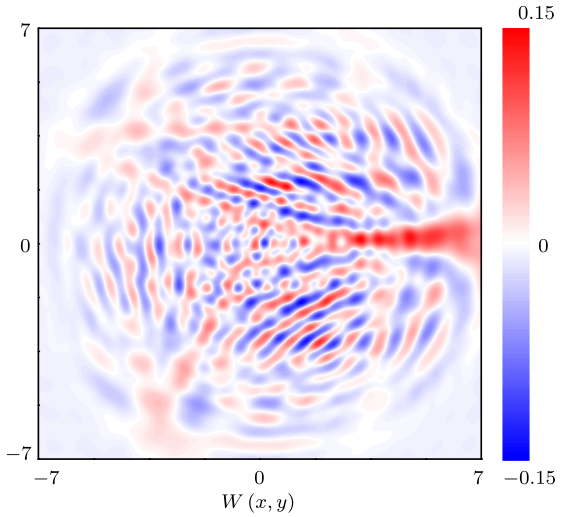

(b) Wigner function

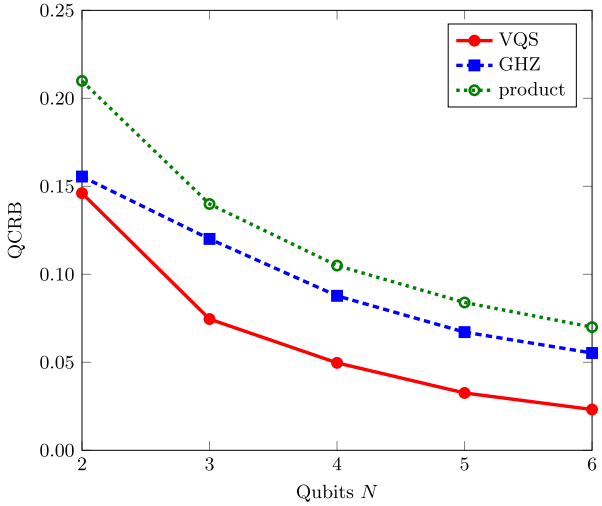

(c) QCRB

Fig. 3. Genetic VQS probe state $|\psi(\boldsymbol{\theta}_\star)\rangle$ for scalar magnetic-field sensing ($N = 6$) under dephasing noise with the same parameters as in Fig. 2.

Fig. 5 shows the QFI $J_\eta(|\psi\rangle)$ for scalar magnetic-field sensing as a function of t seconds under quantum noise as in Figs. 2–4. The maximum value of QFI represents the fundamental sensitivity the quantum state can achieve. The required time to reach this value is an important parameter in quantum sensing, especially in noisy and time-critical scenarios. Generally, the maximum achievable QFI should be acquired quickly to enable faster, more precise, and more efficient parameter estimation. Therefore, the metrological precision of noisy quantum sensing can be comparatively evaluated by analyzing temporal dynamics of QFI for respective probe states. We can see from Fig. 5(a) and 5(b) that the VQS probe state reaches its larger QFI peak at a negligibly delayed time than the GHZ or product states, as expected. Fig. 5(a) shows a negligible QFI difference for VQS and GHZ states under bit-flip and dephasing noises, while the product probe state peaks at a delayed time with a large value in dephasing noise. The GHZ probe state peaks marginally faster, while the VQS state attains a notably higher maximum QFI. Solving the Lindblad master equation is not trivial. Therefore, we first consider the case where the Hamiltonian that encodes the parameter commutes with the decay operator, allowing us to obtain the solution of the Lindblad master equation. Then, we consider the case where the decay operator is assumed to be fixed and the Hamiltonian is changed slightly. As analytically derived in [66] for dephasing noise in estimating the magnetic field in the z-axis direction, where the Hamiltonian and the decay operator commute, the performance of the GHZ state degrades N time faster compared to the product state. Hence, when the Hamiltonian encoding the parameter is slightly changed so that the Hamiltonian no longer commutes with the decay operator, we expect the GHZ state performance to degrade even faster compared to the product state, with the performance degradation limit being N times faster when the Hamiltonian and decay operator commute. Since bit-flip noise can be viewed as dephasing noise in a different basis, this behavior is also expected under bit-flip noise. Moreover, there exists a state that can achieve better performance than the GHZ state, which can be obtained variationally using the VQS probe state [66]. As seen from Fig. 5(b), the time difference to reach peak QFI is negligible, but the maximum values significantly vary in the order of VQS, product, and GHZ probe states under the amplitude damping noise. Figs. 5(c) and 5(d) show the QFI achieved by VQS probe states under bit-flip, dephasing, and amplitude-dampling noises when $N = 2, 3, 4, 5$, and 6. As the number N of qubits increases, the maximum achievable QFI

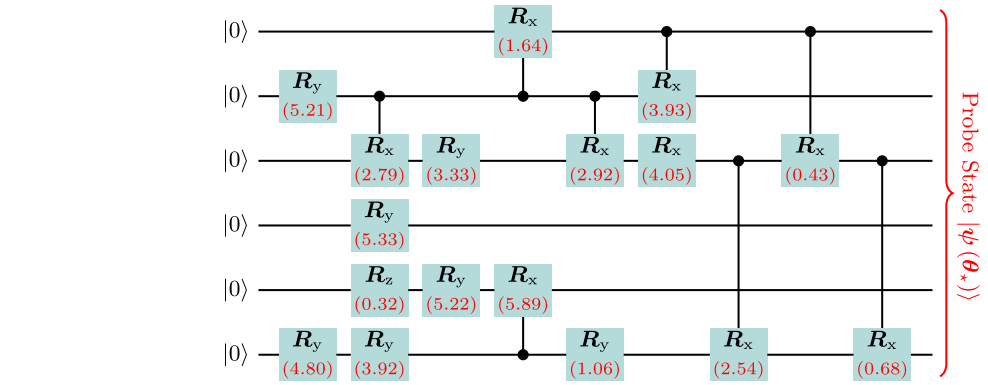

(a) Optimized PQC

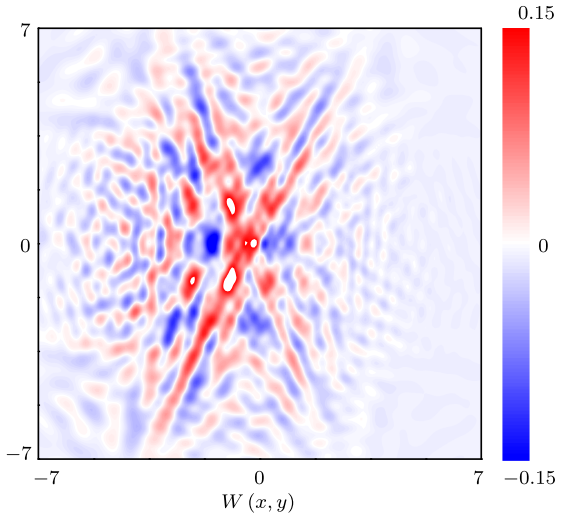

(b) Wigner function

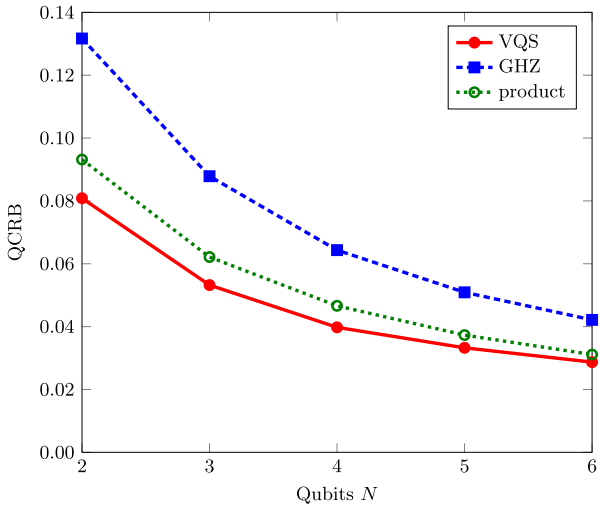

(c) QCRB

Fig. 4. Genetic VQS probe state $|\psi(\boldsymbol{\theta}_\star)\rangle$ for scalar magnetic-field sensing ($N = 6$) under amplitude-damping noise with the same parameters as in Fig. 2.

notably increases, while the time to reach its peak decreases slightly under bit-flip and dephasing noises or remains largely unchanged for amplitude-damping noise. We can also see from Fig. 5(c) that the QFI difference under bit-flip and dephasing noise nearly vanishes as N increases.

3) Vector Magnetic-Field Sensing: To sense all the magnetic field components, multiparameter sensing is employed for simultaneous parameter estimation. In contrast to using qubits for individual component estimation, this method leverages all the qubits at once, offering improved precision. The optimal probe state for simultaneously estimating all magnetic field components is not as well established as in the single-parameter case. Using a single- or two-qubit system, the GHZ state is optimal for two-dimensional magnetic-field sensing. However, the GHZ state may not be optimal for larger systems. For the three-dimensional magnetic field, the GHZ state even leads to a singular QFIM for one or two qubits.

Since the Pauli operators $\boldsymbol{\sigma}_\mathrm{x}$,$\boldsymbol{\sigma}_\mathrm{y}$, and $\boldsymbol{\sigma}_\mathrm{z}$ are *traceless* and have -1 *determinant*, the eigenvalues of each Pauli operator are equal to ± 1. Let $|\pm 1\rangle_\mathrm{v}$ be the normalized eigenvectors corresponding to eigenvalues ± 1 for the Pauli operator $\boldsymbol{\sigma}_\mathrm{v}$ for $\mathrm{v} \in \{\mathrm{x}, \mathrm{y}, \mathrm{z}\}$. The eigenvectors of the Pauli operators $\boldsymbol{\sigma}_\mathrm{x}$ and $\boldsymbol{\sigma}_\mathrm{y}$ are linear combinations of the eigenvectors of $\boldsymbol{\sigma}_\mathrm{z}$ and $\boldsymbol{\sigma}_\mathrm{x}$, respectively, as follows:

$$|\pm 1\rangle_\mathrm{x} = |\pm\rangle \tag{49}$$

$$|\pm 1\rangle_\mathrm{y} = \frac{|+\rangle \mp \imath\,|-\rangle}{\sqrt{2}} \tag{50}$$

$$|\pm 1\rangle_\mathrm{z} = |\tfrac{1}{2}(1 \mp 1)\rangle \tag{51}$$

where $|\pm\rangle = (|0\rangle \pm |1\rangle)/\sqrt{2}$ are the x-basis (Hadamard-basis or bit-flip) states. Let $|\mathsf{ghz}_N\rangle_\mathrm{v}$ be the v-basis GHZ state of N qubits, given by

$$|\mathsf{ghz}_N\rangle_\mathrm{v} = \frac{1}{\sqrt{2}}\left(|+1\rangle_\mathrm{v}^{\otimes N} + |-1\rangle_\mathrm{v}^{\otimes N}\right) \tag{52}$$

for $\mathrm{v} \in \{\mathrm{x}, \mathrm{y}, \mathrm{z}\}$. Now, we consider the probe state for the three-dimensional magnetic field with the unnormalized version as follows [67]:

$$|\phi(\boldsymbol{\theta})\rangle = |\mathsf{ghz}_N\rangle_\mathrm{x} + e^{-\imath\theta_1}|\mathsf{ghz}_N\rangle_\mathrm{y} + e^{-\imath\theta_2}|\mathsf{ghz}_N\rangle_\mathrm{z} \tag{53}$$

Then, the normalized probe state is given by

$$|\psi(\boldsymbol{\theta})\rangle = \frac{|\phi(\boldsymbol{\theta})\rangle}{|\langle\phi(\boldsymbol{\theta})|\phi(\boldsymbol{\theta})\rangle|}. \tag{54}$$

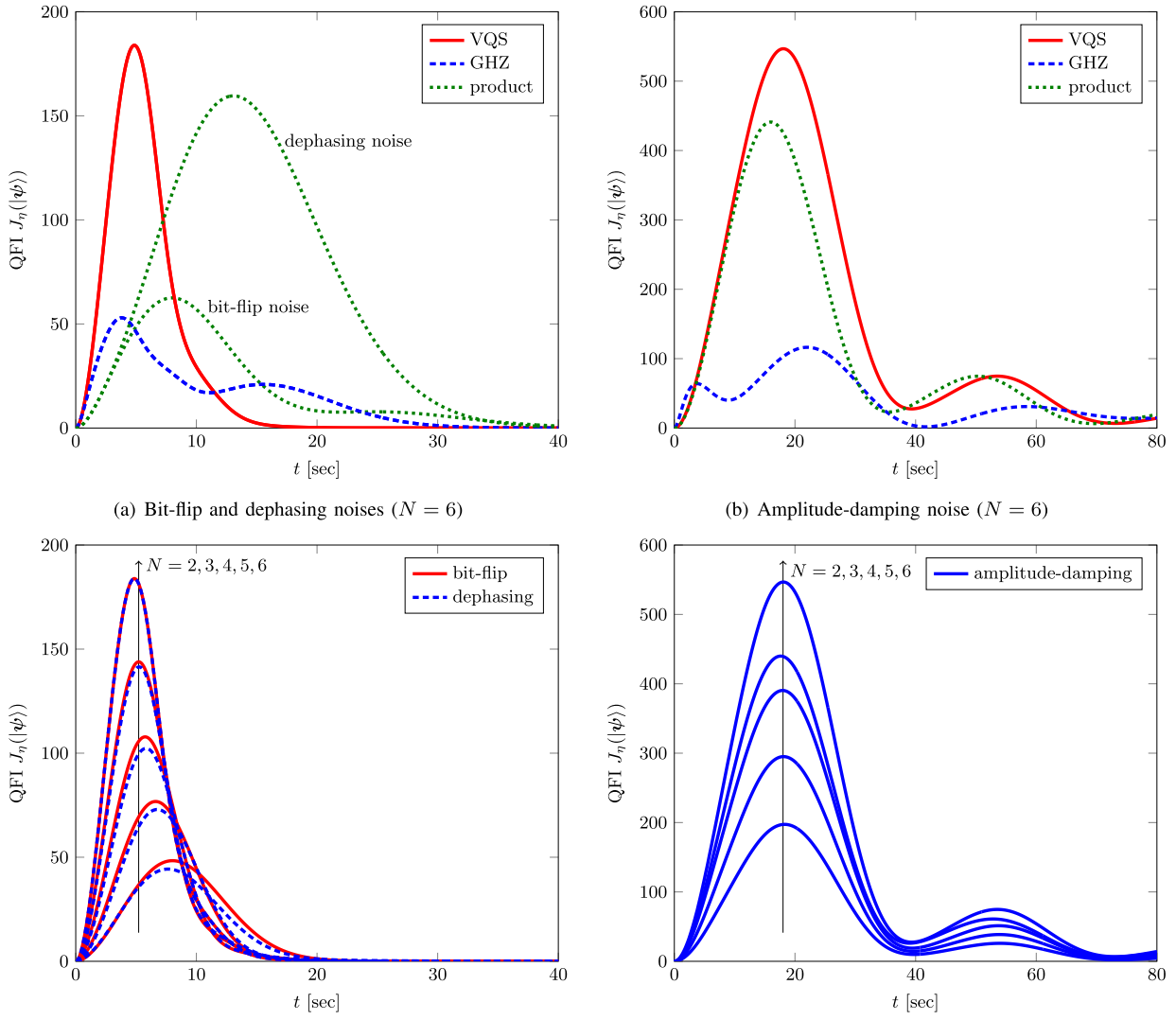

(a) Bit-flip and dephasing noises ($N = 6$)

(b) Amplitude-damping noise ($N = 6$)

(c) VQS states under bit-flip and dephasing noises

(d) VQS states under amplitude-damping noise

Fig. 5. QFI $J_\eta(|\psi\rangle)$ for scalar magnetic-field sensing as a function of t seconds under quantum noise as in Figs. 2–4. The QFI for VQS, GHZ, and product probe states is plotted under (a) bit-flip and dephasing noises and (b) amplitude-damping noise when $N = 6$. In addition, the QFI for the VQS probe state is plotted under (c) bit-flip and dephasing noises and (d) amplitude-damping noise when $N = 2, 3, 4, 5$, and 6.

When $N = 4n$ for a positive integer n, by setting $\boldsymbol{\theta} = (\theta_1, \theta_2)$ to $\boldsymbol{\theta} = \mathbf{0}$, the variance of the estimator is bounded as [67]

$$\sum_{k=1}^{K} \mathrm{Var}\left[\hat{\eta}_k\right] \geq \frac{3 + 6/\mathrm{sinc}^2\left(\|\boldsymbol{\eta}\|\right)}{4N\left(N+2\right)} \tag{55}$$

where $\mathrm{sinc}\left(x\right) = \sin\left(x\right)/x$ and $\|\boldsymbol{\eta}\|$ is not an integer multiple of π. For noisy cases, the purity of the probe state $|\boldsymbol{\psi}\left(\boldsymbol{\theta}\right)\rangle$ is decreased, rendering it to be mixed (which is described by the density matrix $\boldsymbol{\rho}\left(\boldsymbol{\theta}\right)$), and tailored variationally using the PQC designed by the GA. Let

$$\boldsymbol{\rho}\left(\boldsymbol{\theta}\right) = \begin{cases} |\boldsymbol{\psi}\left(\boldsymbol{\theta}\right)\rangle\langle\boldsymbol{\psi}\left(\boldsymbol{\theta}\right)|, & \text{for noiseless} \\ \displaystyle\sum_{i=1}^{2^N} a_i \, |\boldsymbol{\psi}_i\left(\boldsymbol{\theta}\right)\rangle\langle\boldsymbol{\psi}_i\left(\boldsymbol{\theta}\right)|, & \text{for noisy} \end{cases} \tag{56}$$

where $\sum_{i=1}^{2^N} a_i = 1$. Then, the diagonal and off-diagonal entries of the QFIM are approximated from (15) as follows:

$$\left[\boldsymbol{J}_{\boldsymbol{\theta}}(\boldsymbol{\rho})\right]_{kk} \approx 8\left(\frac{1 - \sqrt{\mathcal{F}\left(\boldsymbol{\rho}\left(\boldsymbol{\theta}\right), \boldsymbol{\rho}\left(\boldsymbol{\theta}; \epsilon \boldsymbol{e}_k\right)\right)}}{\epsilon^2}\right) \tag{57}$$

$$\left[\boldsymbol{J}_{\boldsymbol{\theta}}(\boldsymbol{\rho})\right]_{ij} \approx 4\left(\frac{1 - \sqrt{\mathcal{F}\left(\boldsymbol{\rho}\left(\boldsymbol{\theta}\right), \boldsymbol{\rho}\left(\boldsymbol{\theta}; \epsilon \boldsymbol{e}_i + \epsilon \boldsymbol{e}_j\right)\right)}}{\epsilon^2}\right) - \frac{\left[\boldsymbol{J}_{\boldsymbol{\theta}}(\boldsymbol{\rho})\right]_{ii} + \left[\boldsymbol{J}_{\boldsymbol{\theta}}(\boldsymbol{\rho})\right]_{jj}}{2} \tag{58}$$

and $\left[\boldsymbol{J}_{\boldsymbol{\theta}}(\boldsymbol{\rho})\right]_{ij} = \left[\boldsymbol{J}_{\boldsymbol{\theta}}(\boldsymbol{\rho})\right]_{ji}$ due to the symmetric property of the QFIM, where $\boldsymbol{e}_k$ is the row vector of zeros with 1 in the kth position. It has been known that when the noise is aligned with the magnetic field, the probe state in the form of (54) cannot surpass the SQL for a constant decay rate [68].

Numerical Examples: Figs. 6–8 show the QCRBs for vector magnetic-field sensing with the VQS, GHZ, and product probe states when $N = 2, 3, 4, 5$, and 6 under the bit-flip, dephasing, and amplitude-damping noises as in Figs. 2–4. For

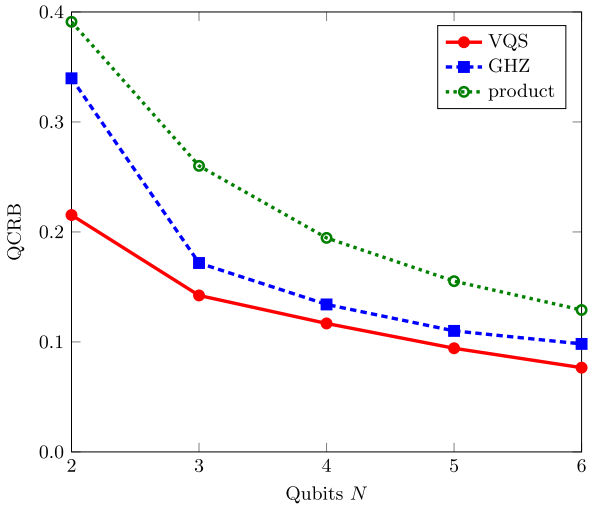

Fig. 6. QCRBs for vector magnetic-field sensing with VQS, GHZ, and product probe states as a function of N under bit-flip noise as in Fig. 2(c).

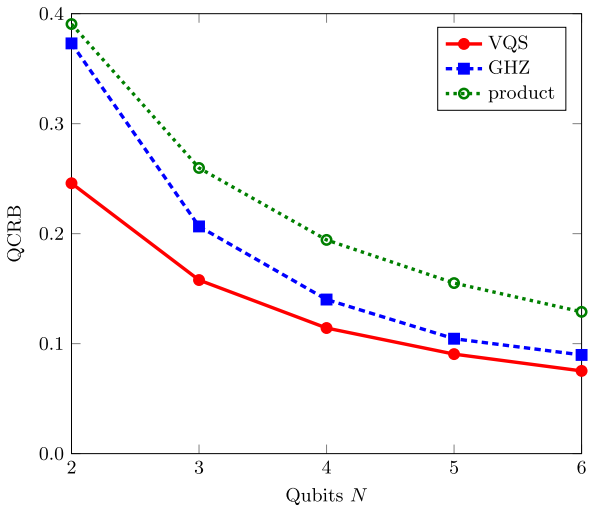

Fig. 7. QCRBs for vector magnetic-field sensing with VQS, GHZ, and product probe states as a function of N under dephasing noise as in Fig. 3(c).

this multiparameter sensing, we set $q = 20$, $r = 3$, and $s = 5$ for the GA to optimize the PQC structure for VQS. We denote (54) by the GHZ state and generate the product state as

$$|\psi(\boldsymbol{\theta})\rangle = \left(\frac{|\phi(\boldsymbol{\theta})\rangle}{|\langle\phi(\boldsymbol{\theta})|\phi(\boldsymbol{\theta})\rangle|}\right)^{\otimes N} \tag{59}$$

where

$$|\phi(\boldsymbol{\theta})\rangle = |\mathsf{ghz}_1\rangle_{\mathrm{x}} + e^{-\imath\theta_1}|\mathsf{ghz}_1\rangle_{\mathrm{y}} + e^{-\imath\theta_2}|\mathsf{ghz}_1\rangle_{\mathrm{z}}. \tag{60}$$

We also optimize the parameters $\boldsymbol{\theta}$ of these GHZ and product states for comparison. Similarly, the VQS probe states show improved precision bounds for all three types of noise, and all the probe states are more robust against amplitude-damping noise. The bit-flip and dephasing noises degrade the QCRB in a comparable way and the GHZ state is more robust than the product state in these types of noise. In contrast, the product probe state is more robust than the GHZ state in the amplitude-damping noise.

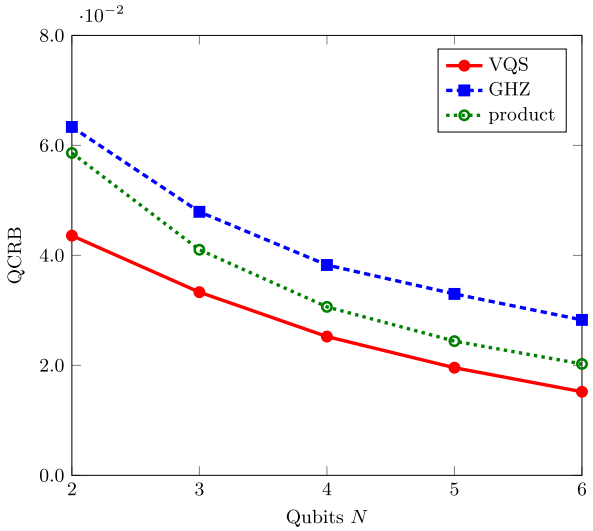

Fig. 8. QCRBs for vector magnetic-field sensing with VQS, GHZ, and product probe states as a function of N under amplitude-damping noise as in Fig. 4(c).

B. QAS Broadcast

To anonymously share the sensing information obtained by VQS among all the sensors in the QAS network, we employ the QAB protocol that ensures anonymity and untraceability in the broadcast process even when the global quantum state is completely known to other sensors.

1) QAB Protocol: The QAB protocol allows any network sensor to anonymously broadcast its sensing information without revealing its identity. To modulate (encode) the information $\mathsf{b} \in \mathbb{Z}_2 = \{0, 1\}$ on its qubit, the broadcasting sensor flips the x-basis state by applying $\boldsymbol{\sigma}_{\mathrm{x}}^{\mathsf{b}}$. Specifically, the QAB protocol takes a series of steps as follows (see Fig. 9).

Broadcast Preparation: The QAS broadcast protocol starts by preparing an M-qubit GHZ-type state in the x-basis that is shared among all sensor nodes. The M-qubit (z-basis) GHZ state is generated from the state $|0\rangle^{\otimes M}$ as

$$|\mathsf{ghz}_M\rangle_{\mathrm{z}} = \boldsymbol{G}_M \cdots \boldsymbol{G}_2 \boldsymbol{G}_1 |0\rangle^{\otimes M}. \tag{61}$$

After the z-basis GHZ state is shared among all M sensors, each sensor applies the Hadamard operator $\boldsymbol{H}$ to its qubit to prepare the x-basis GHZ state as follows:

$$\begin{aligned}|\mathsf{ghz}_M\rangle_{\mathrm{x}} &= \boldsymbol{H}^{\otimes M}|\mathsf{ghz}_M\rangle_{\mathrm{z}} \\ &= \frac{1}{\sqrt{2}}\left(|+\rangle^{\otimes M} + |-\rangle^{\otimes M}\right) \\ &= \frac{1}{\sqrt{2^{M+1}}}\sum_{\boldsymbol{x}\in\mathbb{Z}_2^M}\left(|\boldsymbol{x}\rangle + (-1)^{\mathrm{sum}_2(\boldsymbol{x})}|\boldsymbol{x}\rangle\right) \\ &= \frac{1}{\sqrt{2^{M-1}}}\sum_{\boldsymbol{x}\in\mathbb{Z}_2^M(0)}|\boldsymbol{x}\rangle \end{aligned} \tag{62}$$

where $\mathbb{Z}_2^M(b)$ represents the set of M-tuple binary sequences (or vectors) with $\mathrm{sum}_2(\boldsymbol{x}) = b \in \mathbb{Z}_2$ and

$$\mathrm{sum}_2(\boldsymbol{x}) = \sum_{j=1}^{M} x_j \mod 2 \tag{63}$$

denotes the modulo 2 addition of all the elements in the binary sequence (or vector) $\boldsymbol{x} = (x_1, x_2, \ldots, x_M) \in \mathbb{Z}_2^M$.

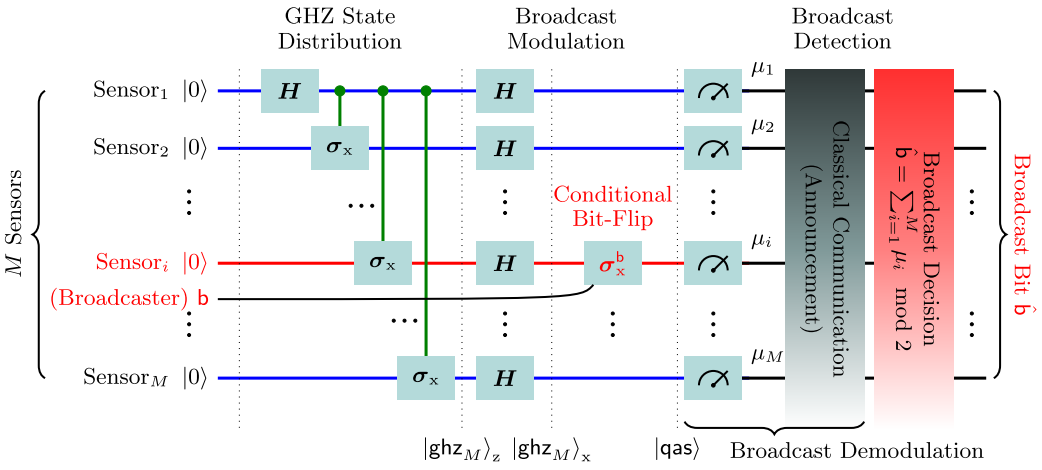

Fig. 9. QAB protocol for QAS broadcast.

Broadcast Modulation: Let the ith sensor want to broadcast its sensing information $\mathsf{b} \in \mathbb{Z}_2$ to all the network sensors, where $i \in \{1, 2, \ldots, M\}$. Then, the ith sensor modulates the broadcast bit b on its qubit by performing the conditional bit-flip Pauli $\boldsymbol{\sigma}_{\mathrm{x}}^{\mathsf{b}}$. This broadcast modulation transforms the x-basis GHZ state to the QAS broadcast state

$$|\mathsf{qas}\rangle = \boldsymbol{X}_{i,M}^{\mathsf{b}} |\mathsf{ghz}_M\rangle_{\mathrm{x}} = \frac{1}{\sqrt{2^{M-1}}} \sum_{\boldsymbol{x} \in \mathbb{Z}_2^M(\mathsf{b})} |\boldsymbol{x}\rangle . \tag{64}$$

Note that the modulated state $|\mathsf{qas}\rangle$ is in the even superposition of all $|\boldsymbol{x}\rangle = |x_1 x_2 \cdots x_M\rangle$ with the modulo 2 sum equal to the broadcast information b. Since this broadcast-modulated state does not depend on the sensor index i and completely hides the broadcasting sensor's identity, the protocol ensures anonymity and untraceability in the QAS network.

Broadcast Detection: All the M network sensors measure their respective qubits in the computational basis and obtain binary measurement outcomes $\mu_1, \mu_2, \ldots, \mu_M$. This M-tuple binary outcome sequence $\boldsymbol{\mu} = (\mu_1, \mu_2, \ldots, \mu_M) \in \mathbb{Z}_2^M$ appears randomly with an equal probability of $1/2^{M-1}$ due to the x-basis change from the Hadamard operations. However, the modulo sum of all these measurement outcomes is equal to the broadcast sensing information b, i.e., $\mathrm{sum}_2(\boldsymbol{\mu}) = \mathsf{b}$—by the symmetry of the state $|\mathsf{qas}\rangle$ due to the bit-flip modulation. Now, all network sensors announce their measurement outcomes by classical communication. Finally, all $M-1$ recipient sensors recover the sensing information with probability 1 as

$$\hat{\mathsf{b}} = \mathrm{sum}_2(\boldsymbol{\mu}) \tag{65}$$

without revealing the identity of the broadcasting sensor.

2) Noisy Broadcast: We analyze the QAB error probability in noisy QSNs, where each qubit of the M-partite GHZ state $|\mathsf{ghz}_M\rangle_{\mathrm{z}}$ possessed by quantum sensors is subject to the local quantum noise. Again, using (41)–(47), we consider the well-known anisotropic quantum noise described by the CPTP map in the Kraus operator-sum representation as follows:

$$\mathcal{N}(\boldsymbol{\rho}) = \boldsymbol{E}_0 \boldsymbol{\rho} \boldsymbol{E}_0^\dagger + \boldsymbol{E}_1 \boldsymbol{\rho} \boldsymbol{E}_1^\dagger \tag{66}$$

where Kraus operators $\boldsymbol{E}_0 = \sqrt{1-p/2}\boldsymbol{I}$ and $\boldsymbol{E}_1 = \sqrt{p/2}\boldsymbol{\sigma}_{\mathrm{x}}$ for bit-flip noise $\mathcal{N} = \mathcal{N}_X$; $\boldsymbol{E}_0 = \sqrt{1-p/2}\boldsymbol{I}$ and $\boldsymbol{E}_1 = \sqrt{p/2}\boldsymbol{\sigma}_{\mathrm{z}}$ for dephasing noise $\mathcal{N} = \mathcal{N}_Z$; $\boldsymbol{E}_0 = |0\rangle\langle 0| + \sqrt{1-p}\,|1\rangle\langle 1|$ and $\boldsymbol{E}_1 = \sqrt{p}\,|0\rangle\langle 1|$ for amplitude-damping noise; and $p \in [0,1]$ denotes a noise parameter such that the qubit is *bit-flipped*, *phase-flipped* with probability $p/2$, or *amplitude-damped* (i.e., decaying from state $|1\rangle$ to $|0\rangle$) with probability p while left untouched (no error) with the complementary probability. Note that the noise parameter p in Kraus operators is related to the decay rate for the ith qubit γ_i in the Lindblad master equation as follows:

$$p = \begin{cases} 1 - e^{-2\gamma_i t}, & \text{bit-flip, dephasing} \\ 1 - e^{-\gamma_i t}, & \text{amplitude-damping.} \end{cases} \tag{67}$$

The broadcast BEP for the QAB protocol under quantum noise $\mathcal{N}$ that acts on each qubit is given by

$$P_{\mathrm{b}}(\mathcal{N}) = \sum_{i \in \mathbb{Z}_2} \Pr\left[\hat{\mathsf{b}} \neq \mathsf{b} \middle| \mathsf{b} = i, \boldsymbol{\rho}(\mathcal{N})\right] \Pr[\mathsf{b} = i] \tag{68}$$

$$= \begin{cases} 0, & \text{bit-flip} \\ \frac{1}{2} - \frac{1}{2}(1-p)^M, & \text{dephasing} \\ \frac{1}{2} - \frac{1}{2}(1-p)^{M/2}, & \text{amplitude-damping} \end{cases} \tag{69}$$

where all derivations are relegated to the Appendix and

$$\boldsymbol{\rho}(\mathcal{N}) = \mathcal{N}^{\otimes M}\left(|\mathsf{ghz}_M\rangle_{\mathrm{z}}\langle \mathsf{ghz}_M|\right) = \frac{1}{2} \sum_{i,j \in \mathbb{Z}_2} \mathcal{N}\left(|i\rangle\langle j|\right)^{\otimes M} \tag{70}$$

is the noisy z-basis GHZ state prepared for the QAS broadcast. Note that the *error-free* resilience of the QAB protocol under bit-flip noise is due to the fact that this noise leaves the qubit's phase unchanged, only bit-flipping its state. Projecting $|i\rangle\langle j|$ in x-basis is equal to projecting the bit-flipped version of $|i\rangle\langle j|$ in x-basis, i.e., $\langle \pm|\boldsymbol{\sigma}_{\mathrm{x}}|i\rangle\langle j|\boldsymbol{\sigma}_{\mathrm{x}}|\pm\rangle = \langle \pm|i\rangle\langle j|\pm\rangle$, since $|\pm\rangle$ are the eigenvectors of $\boldsymbol{\sigma}_{\mathrm{x}}$ corresponding to ± 1 eigenvalues.

In the low-noise regime, the QAB error probability $P_{\mathrm{b}}(\mathcal{N})$ behaves as

$$P_{\mathrm{b}}(\mathcal{N}) = p\mathcal{S}_0 + o(p) \qquad (p \to 0) \tag{71}$$

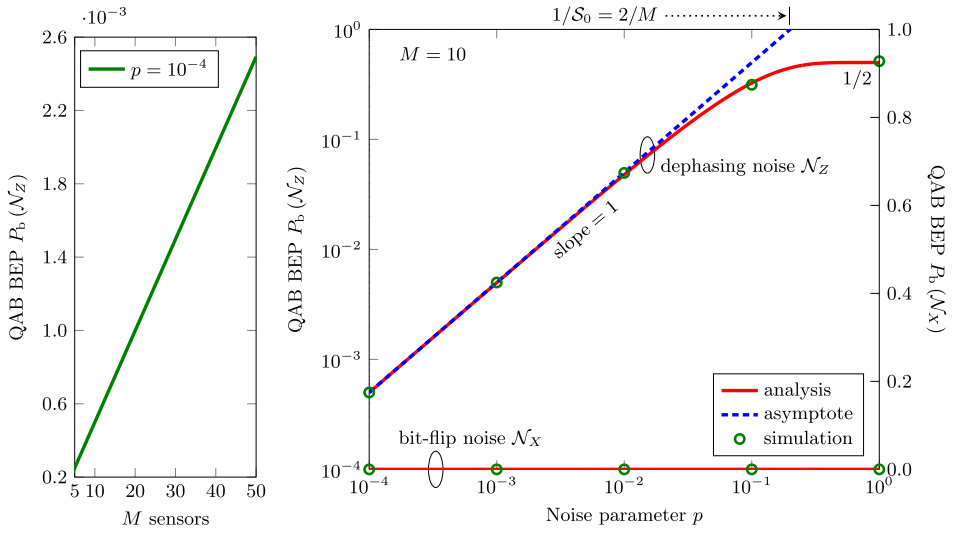

Fig. 10. Broadcast BEP $P_{\mathrm{b}}(\mathcal{N})$ for the QAB protocol as a function of the noise parameter p when $M = 10$ (right) and as a function of the number M of sensing nodes when $p = 10^{-4}$ (left) under bit-flip noise $\mathcal{N}_X$ and dephasing noise $\mathcal{N}_Z$. For simulations, we use the NetSquid designed for quantum network simulations.

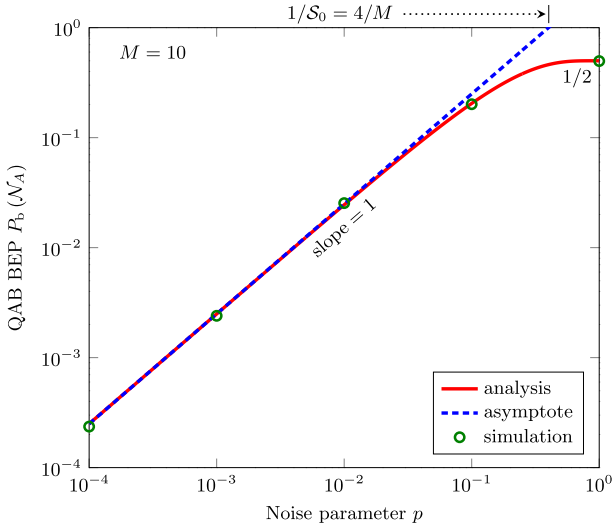

Fig. 11. Broadcast BEP $P_{\mathrm{b}}(\mathcal{N}_A)$ for the QAB protocol as a function of the noise parameter p under amplitude-damping noise $\mathcal{N}_A$ when $M = 10$.

where

$$\mathcal{S}_0 = \lim_{p\to 0} \frac{P_{\mathrm{b}}(\mathcal{N})}{p} = \begin{cases} M/2, & \text{dephasing} \\ M/4, & \text{amplitude-damping.} \end{cases} \tag{72}$$

This asymptotic BEP behavior reveals that the low-noise slope of $P_{\mathrm{b}}(\mathcal{N})$ as a function of p in a log-log plot is equal to one, while the quantity $1/\mathcal{S}_0$ represents the low-noise offset in the BEP asymptote as $p \to 0$—that is, $P_{\mathrm{b}}(\mathcal{N})$ scales linearly with the dephasing or damping probability p and the network size M in the low-noise regime (see Figs. 10 and 11). The coefficient of $1/2$ in each error probability reflects the dimensionality of the quantum system used in the QAB protocol. Since the protocol utilizes a qubit, a two-level system, the coefficient is $1/2$. The difference between the two cases arises from the Kraus operators modeling each noisy channel. For the amplitude-damping channel, the Kraus operator $\boldsymbol{E}_1 = \sqrt{p}\,|0\rangle\langle 1|$ results in the terms $(1-p)^{M/2}$ in the derivation of $P_{\mathrm{b}}(\mathcal{N})$. In contrast, for the dephasing channel, the Kraus operator $\boldsymbol{E}_1 = \sqrt{p/2}\boldsymbol{\sigma}_{\mathrm{z}}$ contributes to the terms $(1-p)^M$. Since the exponent dominates in the low probability regime, this leads to a factor of two difference in the asymptotic behavior between dephasing and amplitude-damping channels.

VI. Conclusion

Emerging applications in wireless networks demand ultra-precise and ultra-secure ISAC solutions. Quantum advantages improve classical precision scaling and provide unconditional security. However, near-term quantum devices face practical challenges, such as inherent quantum noise that hinders their achievable potential. In this paper, we have developed genetic VQS to optimize sensing configurations variationally and evolutionarily in noisy environments. The employed GA approach finds the fittest PQC structure that effectively combats quantum noise, such as bit-flip, dephasing, and amplitude-damping noises. The PQC parameters are adjusted to create a high-quality variational sensing probe state that maximizes the QFI in resilience to quantum noise for both single-parameter and multiparameter sensing. Moreover, we integrate the QAB protocol into VQS networks to anonymously share sensing information among all network parties, ensuring anonymity and untraceability of sensing data. This QAS broadcast has error-free resilience against the bit-flip noise, while its asymptotic BEP linearly scales with the network size and the dephasing or damping probability under dephasing and amplitude-damping noises in the low-noise regime. This work serves to put forth the NISQ ISAC framework specifically in a variational and anonymous manner.

Appendix
Broadcast Error Probability

Due to symmetry, the broadcast BEP $P_{\mathrm{b}}(\mathcal{N})$ in (68) for equiprobable *a priori* broadcast information, i.e., $\Pr[\mathsf{b}=0] = \Pr[\mathsf{b}=1] = 1/2$, can be written as

$$P_{\mathrm{b}}(\mathcal{N}) = \Pr\left[\hat{\mathsf{b}} = 1 \middle| \mathsf{b} = 0, \boldsymbol{\rho}(\mathcal{N})\right]. \tag{73}$$

Hence, only the case $\mathsf{b} = 0$ is considered in deriving the BEP, for which the QAB modulation and demodulation are equivalent to measuring M qubits of the noisy state $\boldsymbol{\rho}(\mathcal{N})$ *locally* in x-basis and calculating the modulo sum of outcomes $\boldsymbol{\mu} \in \mathbb{Z}_2^M$, i.e., $\mathrm{sum}_2(\boldsymbol{\mu})$. If the qubit collapses to $|+\rangle$ or $|-\rangle$, the x-basis measurement outcome is 0 or 1.

A. Bit-Flip Noise

The x-basis projection and bit-flip noise map $\mathcal{N}_X$ of $|i\rangle\langle j|$ for $i, j \in \mathbb{Z}_2$ are given by

$$\langle \pm|i\rangle\langle j|\pm\rangle = (-1)^{i\mp j}\, 1/2 \tag{74}$$

$$\mathcal{N}_X(|i\rangle\langle j|) = (1-p/2)\,|i\rangle\langle j| + p/2\,|1-i\rangle\langle 1-j|\,. \tag{75}$$

Using (70), (74), and (75), the measurement outcome probability of $\boldsymbol{\mu} \in \mathbb{Z}_2^M(0)$ for the bit-flip noisy GHZ state is

$$\Pr\left[\boldsymbol{\mu} \in \mathbb{Z}_2^M(0)\,\middle|\,\boldsymbol{\rho}(\mathcal{N}_X)\right] = \frac{1}{2^{M-1}}. \tag{76}$$

Hence, with 2^{M-1} possible sequences, the broadcast detecting probability under bit-flip noise $\mathcal{N}_X$ is found to be

$$\Pr\left[\mathrm{sum}_2(\boldsymbol{\mu}) = 0 \middle| \mathsf{b} = 0, \boldsymbol{\rho}(\mathcal{N}_X)\right] = 1, \tag{77}$$

leading to the zero BEP in the first case of (69).

B. Dephasing Noise

Using (70), (74), and the dephasing noise maps $\mathcal{N}_Z$ of diagonal $|i\rangle\langle i|$ and non-diagonal $|i\rangle\langle 1-i|$ states

$$\mathcal{N}_Z(|i\rangle\langle i|) = |i\rangle\langle i| \tag{78}$$

$$\mathcal{N}_Z(|i\rangle\langle 1-i|) = (1-p)\,|i\rangle\langle 1-i| \tag{79}$$

for $i \in \mathbb{Z}_2$, we have

$$\Pr\left[\boldsymbol{\mu} \in \mathbb{Z}_2^M(0)\,\middle|\,\boldsymbol{\rho}(\mathcal{N}_Z)\right] = \frac{1+(1-p)^M}{2^M}. \tag{80}$$

Again, with 2^{M-1} possible sequences, the broadcast detecting probability under dephasing noise $\mathcal{N}_Z$ is as follows:

$$\Pr\left[\mathrm{sum}_2(\boldsymbol{\mu}) = 0 \middle| \mathsf{b} = 0, \boldsymbol{\rho}(\mathcal{N}_Z)\right] = \frac{1+(1-p)^M}{2} \tag{81}$$

leading to the broadcast BEP in the second case of (69).

C. Amplitude-Damping Noise

Similarly, since the amplitude-damping noise maps $\mathcal{N}_A$ of diagonal $|i\rangle\langle i|$ and non-diagonal $|i\rangle\langle 1-i|$ states for $i \in \mathbb{Z}_2$ are given by

$$\mathcal{N}_A(|0\rangle\langle 0|) = |0\rangle\langle 0| \tag{82}$$

$$\mathcal{N}_A(|1\rangle\langle 1|) = p\,|0\rangle\langle 0| + (1-p)\,|1\rangle\langle 1| \tag{83}$$

$$\mathcal{N}_A(|i\rangle\langle 1-i|) = \sqrt{1-p}\,|i\rangle\langle 1-i|\,, \tag{84}$$

the broadcast detecting probability under amplitude-damping noise $\mathcal{N}_A$ is obtained as

$$\Pr\left[\mathrm{sum}_2(\boldsymbol{\mu}) = 0 \middle| \mathsf{b} = 0, \boldsymbol{\rho}(\mathcal{N}_A)\right] = \frac{1+(1-p)^{M/2}}{2} \tag{85}$$

leading to the QAB BEP in the third case of (69).

REFERENCES

[1] M. Z. Win, Y. Shen, and W. Dai, "A theoretical foundation of network localization and navigation," *Proc. IEEE*, vol. 106, no. 7, pp. 1136–1165, Jul. 2018.

[2] U. Khalid, J. U. Rehman, S. N. Paing, H. Jung, T. Q. Duong, and H. Shin, "Quantum network engineering in the NISQ age: Principles, missions, and challenges," *IEEE Netw.*, vol. 38, no. 1, pp. 112–123, Jan. 2024.

[3] Z. Wang, Z. Liu, Y. Shen, A. Conti, and M. Z. Win, "Location awareness in beyond 5G networks via reconfigurable intelligent surfaces," *IEEE J. Sel. Areas Commun.*, vol. 40, no. 7, pp. 2011–2025, Jul. 2022.

[4] R. Du, C. Chen, B. Yang, N. Lu, X. Guan, and X. Shen, "Effective urban traffic monitoring by vehicular sensor networks," *IEEE Trans. Veh. Technol.*, vol. 64, no. 1, pp. 273–286, Jan. 2015.

[5] F. Tang, X. Chen, M. Zhao, and N. Kato, "The roadmap of communication and networking in 6G for the Metaverse," *IEEE Wireless Commun.*, vol. 30, no. 4, pp. 72–81, Aug. 2023.

[6] Z. Zhu, C. Guo, R. Bao, M. Chen, W. Saad, and Y. Yang, "Positioning using visible light communications: A perspective arcs approach," *IEEE Trans. Wireless Commun.*, vol. 22, no. 10, pp. 6962–6977, Oct. 2023.

[7] M. Cheng, Q. Guan, F. Ji, J. Cheng, and Y. Chen, "Dynamic-detection-based trajectory planning for autonomous underwater vehicle to collect data from underwater sensors," *IEEE Internet Things J.*, vol. 9, no. 15, pp. 13168–13178, Aug. 2022.

[8] L. Bai, Y. Yang, Z. Zhang, C. Feng, C. Guo, and J. Cheng, "A high-coverage camera assisted received signal strength ratio algorithm for indoor visible light positioning," *IEEE Trans. Wireless Commun.*, vol. 20, no. 9, pp. 5730–5743, Sep. 2021.

[9] A. Liu et al., "A survey on fundamental limits of integrated sensing and communication," *IEEE Commun. Surveys Tuts.*, vol. 24, no. 2, pp. 994–1034, 2nd Quart., 2022.

[10] T. Van Nguyen, Y. Jeong, H. Shin, and M. Z. Win, "Machine learning for wideband localization," *IEEE J. Sel. Areas Commun.*, vol. 33, no. 7, pp. 1357–1380, Jul. 2015.

[11] Q. N. Le, V.-D. Nguyen, O. A. Dobre, and H. Shin, "RIS-assisted full-duplex integrated sensing and communication," *IEEE Wireless Commun. Lett.*, vol. 12, no. 10, pp. 1677–1681, Oct. 2023.

[12] U. Demirhan and A. Alkhateeb, "Integrated sensing and communication for 6G: Ten key machine learning roles," *IEEE Commun. Mag.*, vol. 61, no. 5, pp. 113–119, May 2023.

[13] A. Conti, S. Mazuelas, S. Bartoletti, W. C. Lindsey, and M. Z. Win, "Soft information for Localization-of-Things," *Proc. IEEE*, vol. 107, no. 11, pp. 2240–2264, Nov. 2019.

[14] M. Z. Win, W. Dai, Y. Shen, G. Chrisikos, and H. V. Poor, "Network operation strategies for efficient localization and navigation," *Proc. IEEE*, vol. 106, no. 7, pp. 1224–1254, Jul. 2018.

[15] F. Meyer et al., "Message passing algorithms for scalable multitarget tracking," *Proc. IEEE*, vol. 106, no. 2, pp. 221–259, Feb. 2018.

[16] Z. Eldredge, M. Foss-Feig, J. A. Gross, S. L. Rolston, and A. V. Gorshkov, "Optimal and secure measurement protocols for quantum sensor networks," *Phys. Rev. A*, vol. 97, no. 4, Apr. 2018, Art. no. 042337.

[17] N. Aslam et al., "Quantum sensors for biomedical applications," *Nature Rev. Phys.*, vol. 5, pp. 157–169, Mar. 2023.

[18] H. Wang et al., "A survey on the metaverse: The state-of-the-art, technologies, applications, and challenges," *IEEE Internet Things J.*, vol. 10, no. 16, pp. 14671–14688, Aug. 2023.

[19] H. Yu, D. Martynov, R. X. Adhikari, and Y. Chen, "Exposing gravitational waves below the quantum sensing limit," *Phys. Rev. D*, vol. 106, no. 6, Sep. 2022, Art. no. 063017.

[20] A. Conti et al., "Location awareness in beyond 5G networks," *IEEE Commun. Mag.*, vol. 59, no. 11, pp. 22–27, Nov. 2021.

[21] F. Zaman, U. Khalid, T. Q. Duong, H. Shin, and M. Z. Win, "Quantum full-duplex communication," *IEEE J. Sel. Areas Commun.*, vol. 41, no. 9, pp. 2966–2980, Sep. 2023.

[22] U. Khalid, M. S. Ulum, A. Farooq, T. Q. Duong, O. A. Dobre, and H. Shin, "Quantum semantic communications for metaverse: Principles and challenges," *IEEE Wireless Commun.*, vol. 30, no. 4, pp. 26–36, Aug. 2023.

[23] M. Z. Win, F. Meyer, Z. Liu, W. Dai, S. Bartoletti, and A. Conti, "Efficient multisensor localization for the Internet of Things: Exploring a new class of scalable localization algorithms," *IEEE Signal Process. Mag.*, vol. 35, no. 5, pp. 153–167, Sep. 2018.

[24] U. Khalid, J. U. Rehman, and H. Shin, "Metrologically resourceful multipartite entanglement under quantum many-body effects," *Quantum Sci. Technol.*, vol. 6, no. 2, Jan. 2021, Art. no. 025007.
[25] G. Wang et al., "Characterizing temperature and strain variations with qubit ensembles for their robust coherence protection," *Phys. Rev. Lett.*, vol. 131, no. 4, Jul. 2023, Art. no. 043602.
[26] K. Yamamoto, S. Endo, H. Hakoshima, Y. Matsuzaki, and Y. Tokunaga, "Error-mitigated quantum metrology via virtual purification," *Phys. Rev. Lett.*, vol. 129, no. 25, Dec. 2022, Art. no. 250503.
[27] Z. Liu, K. K. R. Choo, and J. Grossschadl, "Securing edge devices in the post-quantum Internet of Things using lattice-based cryptography," *IEEE Commun. Mag.*, vol. 56, no. 2, pp. 158–162, Feb. 2018.
[28] F. Zaman, A. Farooq, M. A. Ullah, H. Jung, H. Shin, and M. Z. Win, "Quantum machine intelligence for 6G URLLC," *IEEE Wireless Commun.*, vol. 30, no. 2, pp. 22–30, Apr. 2023.
[29] S. N. Paing et al., "Counterfactual quantum Byzantine consensus for human-centric metaverse," *IEEE J. Sel. Areas Commun.*, vol. 42, no. 4, pp. 905–918, Apr. 2024.
[30] C. D. Marciniak et al., "Optimal metrology with programmable quantum sensors," *Nature*, vol. 603, no. 7902, pp. 604–609, Mar. 2022.
[31] R. Kaubruegger, D. V. Vasilyev, M. Schulte, K. Hammerer, and P. Zoller, "Quantum variational optimization of Ramsey interferometry and atomic clocks," *Phys. Rev. X*, vol. 11, no. 4, Dec. 2021, Art. no. 041045.
[32] H. Huo, M. Zhuang, J. Huang, and C. Lee, "Machine optimized quantum metrology of concurrent entanglement generation and sensing," *Quantum Sci. Technol.*, vol. 7, no. 2, Mar. 2022, Art. no. 025010.
[33] M. Cerezo et al., "Variational quantum algorithms," *Nat. Rev. Phys.*, vol. 3, pp. 625–644, Aug. 2021.
[34] J. Yang, S. Pang, Z. Chen, A. N. Jordan, and A. del Campo, "Variational principle for optimal quantum controls in quantum metrology," *Phys. Rev. Lett.*, vol. 128, no. 16, Apr. 2022, Art. no. 160505.
[35] B. Koczor, S. Endo, T. Jones, Y. Matsuzaki, and S. C. Benjamin, "Variational-state quantum metrology," *New J. Phys.*, vol. 22, no. 8, Aug. 2020, Art. no. 083038.
[36] Y. Zhou, Y. Fang, and Y. Zhang, "Securing wireless sensor networks: A survey," *IEEE Commun. Surveys Tuts.*, vol. 10, no. 3, pp. 6–28, 3rd Quart., 2008.
[37] X. Du and H.-H. Chen, "Security in wireless sensor networks," *IEEE Wireless Commun.*, vol. 15, no. 4, pp. 60–66, Aug. 2008.
[38] A. Khan, U. Khalid, J. U. Rehman, and H. Shin, "Quantum anonymous private information retrieval for distributed networks," *IEEE Trans. Commun.*, vol. 70, no. 6, pp. 4026–4037, Jun. 2022.
[39] A. Khan, U. Khalid, J. U. Rehman, K. Lee, and H. Shin, "Quantum anonymous collision detection for quantum networks," *EPJ Quantum Technol.*, vol. 8, no. 1, p. 27, Dec. 2021.
[40] F. Zaman, S. N. Paing, A. Farooq, H. Shin, and M. Z. Win, "Concealed quantum telecomputation for anonymous 6G URLLC networks," *IEEE J. Sel. Areas Commun.*, vol. 41, no. 7, pp. 2278–2296, Jul. 2023.
[41] A. Khan, J. U. Rehman, and H. Shin, "Quantum anonymous notification for network-based applications," *Quantum Inf. Process.*, vol. 20, no. 12, p. 397, Nov. 2021.
[42] C. L. Degen, F. Reinhard, and P. Cappellaro, "Quantum sensing," *Rev. Mod. Phys.*, vol. 89, no. 3, Jul. 2017, Art. no. 035002.
[43] J. Liu, J. Chen, X.-X. Jing, and X. Wang, "Quantum Fisher information and symmetric logarithmic derivative via anti-commutators," *J. Phys. A, Math. Theor.*, vol. 49, no. 27, May 2016, Art. no. 275302.
[44] A. J. Baldwin and J. A. Jones, "Efficiently computing the Uhlmann fidelity for density matrices," *Phys. Rev. A*, vol. 107, no. 1, Jan. 2023, Art. no. 012427.
[45] M. Cerezo, A. Sone, J. L. Beckey, and P. J. Coles, "Sub-quantum Fisher information," *Quantum Sci. Technol.*, vol. 6, no. 3, Jun. 2021, Art. no. 035008.
[46] L. Li, Q.-W. Wang, S.-Q. Shen, and M. Li, "Quantum coherence measures based on Fisher information with applications," *Phys. Rev. A*, vol. 103, no. 1, Jan. 2021, Art. no. 012401.
[47] V. Giovannetti, S. Lloyd, and L. Maccone, "Quantum metrology," *Phys. Rev. Lett.*, vol. 96, no. 1, Jan. 2006, Art. no. 010401.
[48] M. Valeri et al., "Experimental multiparameter quantum metrology in adaptive regime," *Phys. Rev. Res.*, vol. 5, no. 1, Feb. 2023, Art. no. 013138.
[49] J. Liu, H. Yuan, X.-M. Lu, and X. Wang, "Quantum Fisher information matrix and multiparameter estimation," *J. Phys. A, Math. Theor.*, vol. 53, no. 2, Dec. 2019, Art. no. 023001.
[50] J. J. Meyer, "Fisher information in noisy intermediate-scale quantum applications," *Quantum*, vol. 5, p. 539, Sep. 2021.
[51] T. J. Proctor, P. A. Knott, and J. A. Dunningham, "Multiparameter estimation in networked quantum sensors," *Phys. Rev. Lett.*, vol. 120, no. 8, Feb. 2018, Art. no. 080501.
[52] A. Kandala et al., "Hardware-efficient variational quantum eigensolver for small molecules and quantum magnets," *Nature*, vol. 549, no. 7671, pp. 242–246, Sep. 2017.
[53] L. Bittel and M. Kliesch, "Training variational quantum algorithms is NP-hard," *Phys. Rev. Lett.*, vol. 127, no. 12, Sep. 2021, Art. no. 120502.
[54] M. Schuld, V. Bergholm, C. Gogolin, J. Izaac, and N. Killoran, "Evaluating analytic gradients on quantum hardware," *Phys. Rev. A*, vol. 99, no. 3, Mar. 2019, Art. no. 032331.
[55] R. Sweke et al., "Stochastic gradient descent for hybrid quantum-classical optimization," *Quantum*, vol. 4, p. 314, Aug. 2020.
[56] D. P. Kingma and J. Ba, "Adam: A method for stochastic optimization," 2017, *arXiv:1412.6980*.
[57] X. Ge, R.-B. Wu, and H. Rabitz, "The optimization landscape of hybrid quantum–classical algorithms: From quantum control to NISQ applications," *Annu. Rev. Control*, vol. 54, pp. 314–323, Nov. 2022.
[58] J. Romero, R. Babbush, J. R. McClean, C. Hempel, P. J. Love, and A. Aspuru-Guzik, "Strategies for quantum computing molecular energies using the unitary coupled cluster ansatz," *Quantum Sci. Technol.*, vol. 4, no. 1, Oct. 2018, Art. no. 014008.
[59] S. Y.-C. Chen, C.-M. Huang, C.-W. Hsing, H.-S. Goan, and Y.-J. Kao, "Variational quantum reinforcement learning via evolutionary optimization," *Mach. Learn., Sci. Technol.*, vol. 3, no. 1, Feb. 2022, Art. no. 015025.
[60] T. Rindell, B. Yenilen, N. Halonen, A. Pönni, I. Tittonen, and M. Raasakka, "Exploring the optimality of approximate state preparation quantum circuits with a genetic algorithm," *Phys. Lett. A*, vol. 475, Jul. 2023, Art. no. 128860.
[61] G. C. Knee, E. Bolduc, J. Leach, and E. M. Gauger, "Quantum process tomography via completely positive and trace-preserving projection," *Phys. Rev. A*, vol. 98, no. 6, Dec. 2018, Art. no. 062336.
[62] S. B. Jäger, T. Schmit, G. Morigi, M. J. Holland, and R. Betzholz, "Lindblad master equations for quantum systems coupled to dissipative bosonic modes," *Phys. Rev. Lett.*, vol. 129, no. 6, Aug. 2022, Art. no. 063601.
[63] Y.-J. Liu and S. Lieu, "Dissipative phase transitions and passive error correction," *Phys. Rev. A*, vol. 109, no. 2, Feb. 2024, Art. no. 022422.
[64] G. O. Samach et al., "Lindblad tomography of a superconducting quantum processor," *Phys. Rev. Appl.*, vol. 18, no. 6, Dec. 2022, Art. no. 064056.
[65] A. Kenfack and K. Yczkowski, "Negativity of the Wigner function as an indicator of non-classicality," *J. Opt. B, Quantum Semiclass. Opt.*, vol. 6, no. 10, pp. 396–404, Aug. 2004.
[66] S. F. Huelga, C. Macchiavello, T. Pellizzari, A. K. Ekert, M. B. Plenio, and J. I. Cirac, "Improvement of frequency standards with quantum entanglement," *Phys. Rev. Lett.*, vol. 79, no. 20, pp. 3865–3868, Nov. 1997.
[67] T. Baumgratz and A. Datta, "Quantum enhanced estimation of a multidimensional field," *Phys. Rev. Lett.*, vol. 116, no. 3, Jan. 2016, Art. no. 030801.
[68] L. B. Ho, H. Hakoshima, Y. Matsuzaki, M. Matsuzaki, and Y. Kondo, "Multiparameter quantum estimation under dephasing noise," *Phys. Rev. A*, vol. 102, no. 2, Aug. 2020, Art. no. 022602.

Muhammad Shohibul Ulum received the B.S. degree in electrical engineering from Bandung Institute of Technology, Bandung, Indonesia, in 2020. He is currently pursuing the Ph.D. degree with the Department of Electronics and Information Convergence Engineering, Kyung Hee University, South Korea. His research interests include quantum information science, quantum computing, and quantum metrology.

Uman Khalid received the B.S. degree in electronics engineering from the Ghulam Ishaq Khan (GIK) Institute, Topi, Pakistan, in 2015, and the Ph.D. degree in electronics engineering from Kyung Hee University, South Korea, in February 2023. Since March 2023, he has been a Post-Doctoral Fellow with the Department of Electronics and Information Convergence Engineering, Kyung Hee University. His research interests include quantum information science, quantum metrology, and quantum networks.

Jason William Setiawan received the B.S. degree in electrical engineering from Bandung Institute of Technology, Indonesia, in 2020. He is currently pursuing the Ph.D. degree in quantum information science with the Department of Electronics and Information Convergence Engineering, Kyung Hee University (KHU), South Korea. His research interests include quantum information science, quantum communication, and quantum networks.

Trung Q. Duong (Fellow, IEEE) is a Canada Excellence Research Chair (CERC) and a Full Professor at Memorial University of Newfoundland, Canada. He is also the adjunct Chair Professor in Telecommunications at Queen's University Belfast, UK and a Research Chair of Royal Academy of Engineering, UK. His current research interests include quantum communications, wireless communications, quantum machine learning, and quantum optimisation.

Dr. Duong has served as an Editor/Guest Editor for the IEEE TRANSACTIONS ON WIRELESS COMMUNICATIONS, IEEE TRANSACTIONS ON COMMUNICATIONS, IEEE TRANSACTIONS ON VEHICULAR TECHNOLOGY, IEEE COMMUNICATIONS LETTERS, IEEE WIRELESS COMMUNICATIONS LETTERS, IEEE WIRELESS COMMUNICATIONS, IEEE *Communications Magazines*, and IEEE JOURNAL ON SELECTED AREAS IN COMMUNICATIONS. He received the Best Paper Award at the IEEE VTC-Spring 2013, IEEE ICC 2014, IEEE GLOBECOM 2016, 2019, 2022, IEEE DSP 2017, IWCMC 2019, 2023, and IEEE CAMAD 2023. He has received the two prestigious awards from the Royal Academy of Engineering (RAEng): RAEng Research Chair (2021-2025) and the RAEng Research Fellow (2015-2020). He is the recipient of the prestigious Newton Prize 2017.

Moe Z. Win (Fellow, IEEE) is a Professor at the Massachusetts Institute of Technology (MIT) and the founding director of the Wireless Information and Network Sciences Laboratory. Prior to joining MIT, he was with AT&T Research Laboratories and with NASA Jet Propulsion Laboratory.

His research encompasses fundamental theories, algorithm design, and network experimentation for a broad range of real-world problems. His current research topics include ultra-wideband systems, network localization and navigation, network interference exploitation, and quantum information science. He has served the IEEE Communications Society as an elected Member-at-Large on the Board of Governors, as elected Chair of the Radio Communications Committee, and as an IEEE Distinguished Lecturer. Over the last two decades, he held various editorial positions for IEEE journals and organized numerous international conferences. He has served on the SIAM Diversity Advisory Committee.

Dr. Win is an elected Fellow of the AAAS, the EURASIP, the IEEE, and the IET. He was honored with two IEEE Technical Field Awards: the IEEE Kiyo Tomiyasu Award (2011) and the IEEE Eric E. Sumner Award (2006, jointly with R. A. Scholtz). His publications, coauthored with students and colleagues, have received several awards. Other recognitions include the MIT Frank E. Perkins Award (2024), the MIT Everett Moore Baker Award (2022), the IEEE Vehicular Technology Society James Evans Avant Garde Award (2022), the IEEE Communications Society Edwin H. Armstrong Achievement Award (2016), the Cristoforo Colombo International Prize for Communications (2013), the Copernicus Fellowship (2011) and the *Laurea Honoris Causa* from the Università degli Studi di Ferrara (2008), and the U.S. Presidential Early Career Award for Scientists and Engineers (2004).

Hyundong Shin (Fellow, IEEE) received the B.S. degree in Electronics Engineering from Kyung Hee University (KHU), Yongin-si, Korea, in 1999, and the M.S. and Ph.D. degrees in Electrical Engineering from Seoul National University, Seoul, Korea, in 2001 and 2004, respectively. During his postdoctoral research at the Massachusetts Institute of Technology (MIT) from 2004 to 2006, he was with the Laboratory for Information Decision Systems (LIDS). In 2006, he joined the KHU, where he is currently a Professor in the Department of Electronic Engineering. His research interests include quantum information science, wireless communication, and machine intelligence.

Dr. Shin received the IEEE Communications Society's Guglielmo Marconi Prize Paper Award (2008) and William R. Bennett Prize Paper Award (2012). He served as the Publicity Co-Chair for the IEEE PIMRC (2018) and the Technical Program Co-Chair for the IEEE WCNC (PHY Track 2009) and the IEEE GLOBECOM (Communication Theory Symposium 2012 and Cognitive Radio and Networks Symposium 2016). He was an Editor of IEEE TRANSACTIONS ON WIRELESS COMMUNICATIONS (2007–2012) and IEEE COMMUNICATIONS LETTERS (2013–2015).